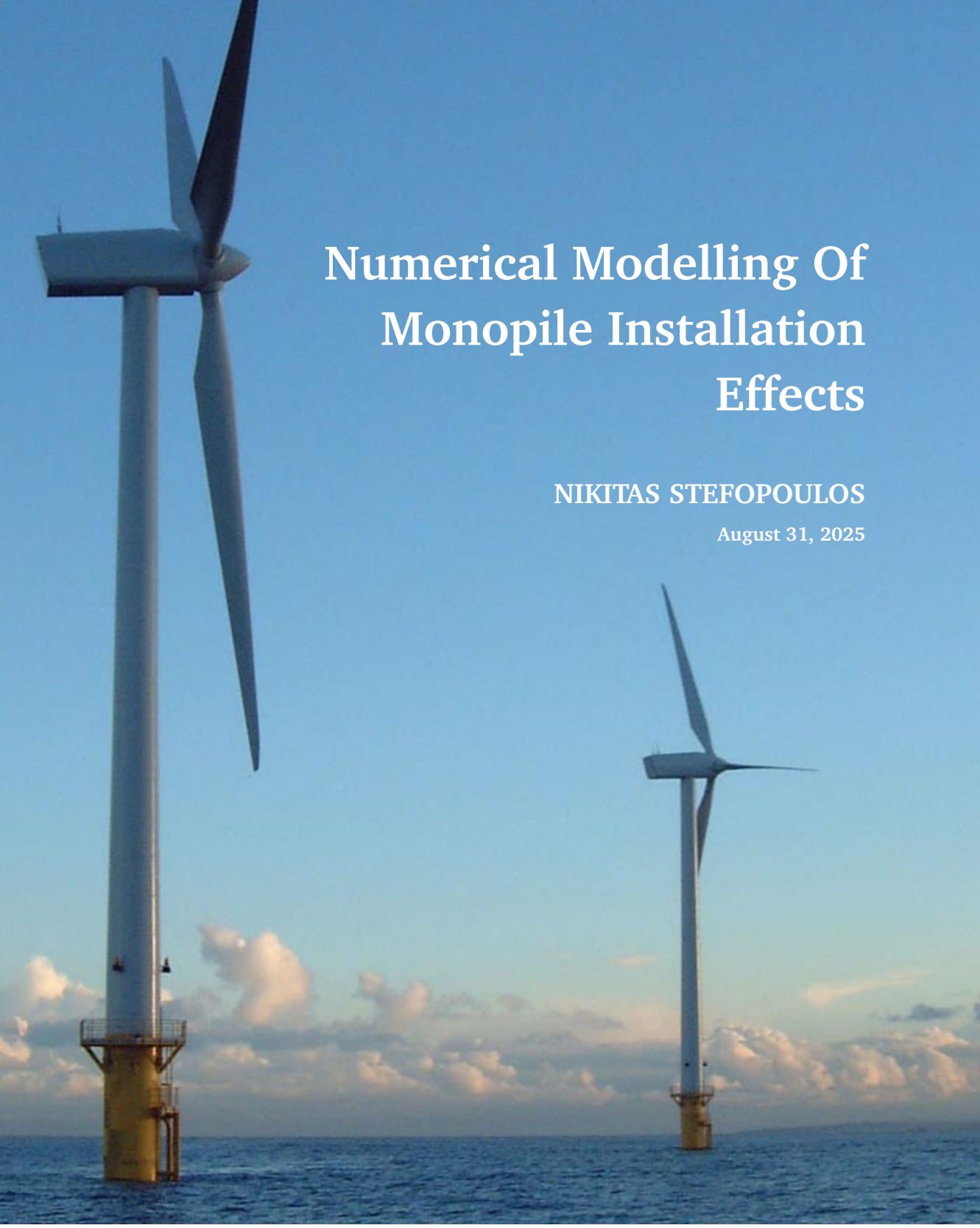

Numerical Modelling Of Monopile Installation Effects

NIKITAS STEFOPOULOS

August 31, 2025

TU Delft Delft University of Technology

SIEMENS energy

Numerical Modelling of Monopile Installation Effects

Master of Science Thesis

Author:	Nikitas Stefopoulos	(Student number: 5440955)
Committee:	Dr. Evangelos Kementzetzidis	TU Delft - Chairman
	Ir. Stavros Panagoulias	Siemens Energy - TU Delft
	Dr. Axel Nernheim	Siemens Energy
	Dr. Federico Pisanò	Norwegian Geotechnical Institute
	Dr. Sandro Brasile	Seequent, the Bentley Subsurface Company
	Dr. Tuan Bui	Seequent, the Bentley Subsurface Company
	Dr. George Lavidas	TU Delft

August 31, 2025

Cover: Offshore windfarm at Blyth, Northumberland, UK. (Image courtesy of AMEC.)

TU Delft Delft University of Technology

SIEMENS energy

Summary

The structural response and thus the service life of offshore wind turbines is significantly affected by their first natural frequency. However, field measurements from offshore wind farms show that the field response of monopile-founded wind turbines is stiffer than expected, suggesting that improved modelling could lead to optimized cost-efficient structures.

This discrepancy may be associated to conservative foundation modelling. The current industry-standard finite element (FE) approach assumes monopiles as wished-in-place (WIP), thus neglecting installation effects. The goal of this thesis is to calibrate a 3D FE model to better capture the lateral response of impact and vibratory-driven monopiles in predominantly sandy soils under monotonic loading, particularly in the small-strain range that governs the dynamic response of offshore wind turbines, by accounting for installation effects.

PLAXIS 3D is used to model the soil-structure interaction with Hardening Soil elastic-plastic constitutive model that can capture small-strain stiffness (HSsmall). The study has a twofold scope: namely, establishing an interpretation scheme for initial soil properties to model the WIP response and incorporating installation effects through a practical approach that captures the effects of the installation on the soil state, and consequently the lateral capacity, without explicitly simulating the pile installation.

The WIP models, validated against a number of field tests, show that the current modelling approach can accurately predict the lateral response of vibratory driven monopiles, while it underestimates the stiffness of impact driven ones. Therefore, this thesis proposes to artificially incorporate installation effects into the established WIP FE models for impact driven monopiles, by either imposing volumetric strains (ϵ_{vol}) to the soil plug or by modifying the coefficient of lateral earth pressure at rest

(K_0). Both methods lead to increased horizontal stresses around the monopile and result in stiffer global response and improved agreement with the field data, for all cases examined.

This thesis offers a comprehensive framework for modelling the lateral response of monotonically loaded monopiles, including installation effects, that could potentially be adopted by industry thanks to its simplicity, computational efficiency and reliance on commonly available data in offshore wind projects.

Acknowledgements

After almost ten, unique, very productive, extremely interesting, sometimes difficult and tiring but above all exciting months, I am very happy to write this final part of my thesis. Graduating within Siemens Energy and studying at TU Delft has been a truly unique experience.

I would like to thank my daily supervisors at Siemens Energy, Stavros and Axel, for their continuous support throughout this thesis project, for spending all this time with me, for helping me understand new concepts, for those really funny sometimes and always productive meetings, but most importantly for inspiring me to work in the field of offshore geotechnics, for being my mentors.

I am also very grateful to my academic supervisor at TU Delft, Vagelis, for the support throughout this journey, for his always valuable feedback and guidance.

My sincere thanks also go to my committee members, Federico, Sandro, and Tuan, for their feedback during the progress meetings and their contribution for shaping and completing this thesis.

At last, I would like to thank my friends, my fellow students and now good friends from Siemens Energy, for the countless hours of ping pong and table soccer, for the always interesting and funny discussions, and for the unforgettable time we shared over these months. And of course a big thank you to my family for always being there for me.

Contents

List of Figures

List of Tables

Nomenclature

Latin symbols

c	Cohesion	kPa
D	Monopile's outer diameter	m
D_r	Relative density	$-$
e	Load eccentricity	m
E_0	Initial small-strain Young's modulus	kPa
E_{50}	Secant stiffness modulus	kPa
E_{oed}	Tangent stiffness modulus	kPa
ϵ_{vol}	Planar volumetric strain	$\%$
E_{ur}	Unloading-reloading stiffness modulus	kPa
f_s	Sleeve friction resistance	MPa
G_0	Initial small-strain shear modulus	kPa
F	Horizontal force	kN
H^*	Dimensionless horizontal force	$-$
K_0	Coefficient of lateral earth pressure at rest	$-$
$K_{0,mod}$	Modified coefficient of lateral earth pressure at rest	$-$
K_0^{NC}	Coefficient of lateral earth pressure at rest for normally consolidated conditions	$-$
K_{sec}	Lateral secant stiffness	MN/m
L	Total monopile's length	m

m	Stress dependency factor	$-$
p	Mean effective stress	kPa
p_{ref}	Reference mean effective stress	kPa
q_c	Cone tip resistance	MPa
s_u	Undrained shear strength	kPa
t	Monopile's wall thickness	m
v^*	Dimensionless horizontal displacement at mudline level	$-$
V_s	Shear wave velocity	MPa
v_t^*	Dimensionless horizontal displacement at sensor level	$-$
z	Distance to the mudline level	m
z_{Bottom}	Soil layer bottom z-coordinate, relative to the mudline level	m
z_{Top}	Soil layer top z-coordinate, relative to the mudline level	m

Greek symbols

α	Exponential decay factor	$-$
β	Stress amplification factor	$-$
γ	Total Unit Weight	kN/m^3
γ'	Effective Unit Weight	kN/m^3
ν	Poisson's ratio	$-$
ν_{ur}	Poisson's ratio of unloading-reloading	$-$
ϕ	Internal Friction Angle	deg
ϕ_{inter}	Interface Friction Angle	deg
ψ	Angle of Dilation	deg
ρ	Density	kg/m^3
σ_1	Major principal stress	kPa
σ_3	Minor principal stress	kPa
σ'_h	Effective horizontal stress	kPa
$\sigma'_{h,post}$	Post-installation effective horizontal stress	kPa

$\sigma'_{h,pre}$	Initial effective horizontal stress	kPa
σ'_{rad}	Effective radial stress	kPa
σ'_{v}	Effective vertical stress	kPa

Subscripts

d	drained
$inter$	interface
u	undrained

Superscripts

ref	reference properties

Abbreviations

1D	One-dimensional
3D	Three-dimensional
A&H	Alm & Hamre
CPT	Cone Penetration Testing
FE	Finite Element
FLS	Fatigue Limit State
HSsmall	Hardening Soil with Small strain stiffness
NC	Normally Consolidated
OC	Overconsolidated
OCR	Overconsolidation ratio
POP	Pre-overconsolidation pressure
PPD	Pile Penetration Depth
SCPT	Seismic Cone Penetration Testing
SLS	Serviceability Limit State
ULS	Ultimate Limit State

WIP	Wished-in-place
WL	Waterline level

Chapter 1

Literature review

1.1 Motivation

Offshore wind energy is continuously expanding and is expected to play a central role in the EU's decarbonisation targets. By 2030, total wind capacity in the EU is projected to reach 351 GW, of which 48 GW will come from offshore wind farms [18]. To ensure the robustness and long-term reliability of these structures, the geotechnical design of the foundation is an integral part of the overall design process, directly influencing the structural response and serviceability.

Most offshore wind farms are located in the shallow waters of the North Sea, where monopiles remain the predominant foundation type due to their simplicity, cost-effectiveness, and suitability for the region's soil and water depth conditions. Field measurements from several bottom-fixed offshore wind farms imply that the natural frequency of wind turbines is consistently higher than expected [21], [32], [39] and [56] as illustrated in Figure 1.1. Moreover, various studies have showcased that the predicted initial stiffness of laterally loaded monopiles by the current engineering practice - either by numerical or analytical modelling - is often significantly underestimated [35]. This discrepancy has been attributed to potentially inaccurate or conservative modelling of this soil-structure interaction problem. A key limitation in the current design practice is that the pile is considered as wished-in-place (WIP), meaning that installation effects are not considered in the model. The aim of this project is to contribute in bridging this frequency gap, from a soil's perspective, by in-

vestigating the influence of installation effects on the lateral response of monopiles, with focus on the initial stiffness.

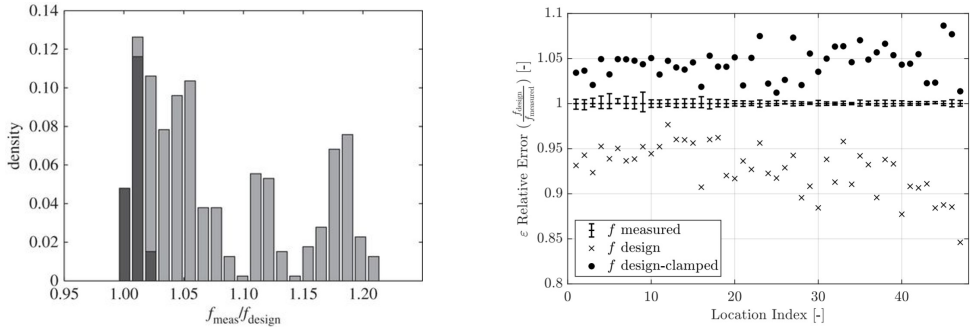

Figure 1.1: Comparison of design and measured natural frequencies. Left: Measured first tower bending frequency (f_{meas}) vs. design frequency (f_{design}) for 400 offshore wind turbines (Kallehave et al. [32]). Right: Relative error between f_{design} and $f_{measured}$ for 47 turbine locations (Nernheim et al. [39]).

1.2 Objective and scope

The objective of this thesis is to improve the prediction of the lateral response of monotonically loaded monopiles, by accounting for installation effects. To achieve this, the finite element software PLAXIS 3D is employed to simulate the soil-structure interaction problem, using the Hardening Soil with small-strain stiffness (HSsmall) constitutive model to adequately capture the non-linear and hardening behaviour of soil. The initial soil parameters are first calibrated based on field and laboratory test data (primarily CPT data) and then the installation effects; namely horizontal stress changes, are artificially incorporated into the model. Therefore instead of modelling the computationally intensive installation process explicitly, its effects are imposed directly onto the model. This approach allows the study to focus on improving the prediction of the lateral response rather than reproducing the installation itself.

The study considers both impact and vibratory driven monopiles in dense, sand dominated sites, where installation effects are expected to be most significant. These conditions are representative of bottom-fixed offshore wind farms in the North Sea region. The analysis focuses on the monotonic lateral response in small strains;

defined as a horizontal displacement of 0.02D at the mudline level, as analytically explained in Section 3.1.

1.3 Lateral response of monopiles

For monopile foundations supporting offshore wind turbines, the dominant design load generally acts laterally [28] and the design is often driven by the fatigue limit state (FLS). In other words, it is the dynamic response, not the ultimate capacity, of the wind turbine that drives the design. However, field measurements show that the measured natural frequency of offshore wind turbines is lower than the designed, suggesting that the current modelling approaches may be further optimized. This frequency gap can be, at least partially, attributed to simplifications in foundation modelling. Factors such as scour protection and installation effects that are usually neglected in foundation modelling are believed to stiffen the actual response and help explain this discrepancy. The latter is also the topic of this thesis; namely how to incorporate installation effects into foundation modelling and make the foundation modelling more accurate.

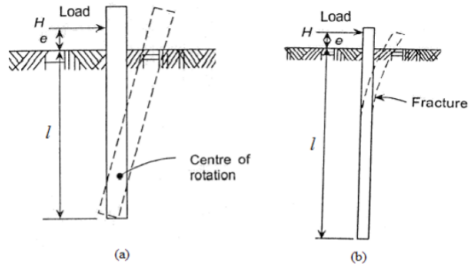

Figure 1.2: Failure mechanism of piles under horizontal load (a) short rigid pile, (b) long slender pile (adapted from [38]).

1.3.1 Current design practice

In engineering practice, soil-structure interaction is simplified to enhance computational efficiency. Traditionally, p-y curves have been used to estimate the lateral response of monopiles. However, these curves that were originally developed for long and slender piles in the in the oil and gas industry, which exhibit “long” failure mechanism characterized by the formation of a plastic hinge and pile bending in the

direction of loading. Such curves tend to underestimate the lateral response of the short, large diameter and rigid monopiles used in offshore wind foundations. These monopiles, with length-to-diameter (L/D) ratios typically below 7 [51], exhibit a "short" failure mechanism [55], where the pile rotates rigidly about a pivot point located below the mudline [11], [29], [50]. The two mechanisms are illustrated in Figure 1.2.

For that reason an extensive joint industry research project (PISA: Pile Soil Analysis) [14] took place in order to improve the accuracy of this method by including more forces in the model to better capture the soil-structure interaction as illustrated in Figure 1.3. Using site specific FE models, revised soil response curves were produced, useful for the design of monopile foundations. In this framework a 1D FE model is used to model the soil structure interaction. The pile is modelled as a Timoshenko beam on elastic foundation.

1.3.2 Soil reaction curves

PISA proposed two calibration approaches for the new p-y curves, a rule-based method and a numerical based, with the latter recommended for detailed design. The numerical approach uses 3D FE models to derive site specific soil reaction curves, which are implemented into 1D FE models to efficiently model the lateral response. The PISA model included additional force components to better capture the lateral pile behaviour. For rigidly rotating piles; such as those used in offshore wind applications, the soil reaction components are illustrated in Figure 1.3.

In addition to lateral distributed forces, the figure shows frictional forces along the pile wall as well as a horizontal shear force and moment at the pile toe. Accurately capturing these of these forces is essential for reliable FE modelling of the lateral response. However for small-strains analyses, as those in this thesis, used for FLS design, studies [41] indicate that the original p-y curves including only the lateral force component, when calibrated against the site-specific 3D FE models, give comparable results to those of the PISA model including all four force components.

1.3.3 Small-strain response

This study focuses on the small-strain response of monopiles under lateral loading that governs the dynamic response of offshore wind turbines. According to Achmus et al. [2] the initial stiffness under monotonic lateral loading can be used as a good approximation of the un- and re-loading stiffness under cyclic loading and can therefore be used for assessing the dynamic response. For that reason this study evaluates

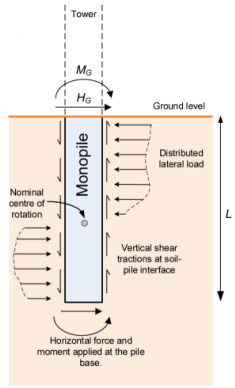

Figure 1.3: Idealization of the soil reaction components acting on a rigidly rotating monopile (Burd et al. [14])

the monotonic lateral behaviour of monopiles at a displacement level up to 2%D at the mudline level. In general, the SLS is defined as a rotation of 0.25 degrees at the mudline [22] which for the slenderness ratios (PPD/D) and pivot depth representative of rigid monopiles used in offshore wind corresponds to a lateral displacement of about 2%D. Project experience indicates that FLS deflection levels remain well below this threshold, while a lateral displacement of 10%D is typically considered the ULS limit. Therefore accurately capturing the initial stiffness in 3D FE modelling will allow for future calibration of the initial stiffness in 1D FE models and therefore improve the prediction accuracy.

The assessment focuses on lateral displacements at the mudline up to 2%D. In general, the SLS is defined as a rotation of 0.25 degrees at the mudline [22] which for the slenderness ratios (PPD/D) and pivot depth characteristic of rigid monopiles used in offshore wind corresponds to a lateral displacement of about 2%D. Project experience indicates that FLS deflection levels remain well below this threshold, while a lateral displacement of 10%D is typically considered the ULS limit.

1.4 Overview of installation methods

Monopiles, open-ended deep steel pile foundations driven into the seabed, are the most common foundation type for offshore wind turbines in shallow waters. As wind turbines become larger, so do the monopiles supporting them, with current design

reaching diameters of up to 11 m diameter and embedment lengths of up to 60 m [31]. Typically the monopiles are installed using impact driving, a well established method from both onshore application but also from the oil and gas industry, where a cyclic axial load is applied at the top of the pile via a hydraulic hammer.

However, the growing size of these steel structures poses new challenges for engineers particularly during installation. The impact driving of large diameter monopiles creates high levels of underwater noise, potentially harmful to marine life [54]. To address this, environmental regulations have been introduced, requiring mitigation measures such as bubble curtains. As a result vibratory driving has gained attention as a quieter and potentially faster alternative. It allows quicker penetration and minimizes the risk of pile run. However, it remains less well understood and currently several ongoing studies examine the soil response during vibratory driving [3], [11], [19], [29].

For both cases; the well established hammering method and for the more recent and not fully investigated vibratory installation, current numerical models might not be accurate enough and underestimate the initial stiffness and lateral capacity of monopiles, leaving room for design optimization and further research.

This thesis investigates installation effects for both techniques. Other more novel installation methods like Gentle Driving of Piles [53] or Vibrojet [12] will not be discussed herein due to their limited technological readiness and the lack of similar applications for the foundation of offshore wind turbines.

1.5 Effects of installation method on the lateral response

The effect of installation on the lateral response is more pronounced in sandy soils. In contrast, current design practices have been found to accurately predict the lateral behaviour of piles in clay [6], [57], [58]. According to Achmus et al. [1] the effect of installation on the bedding resistance is limited in clays compared to non-cohesive soils. Results from the PISA project at Cowden clay showed that the lateral response of monopiles can be accurately captured by WIP FE models, especially for small strains [57], [58]. Alsharedah et al. [6] used PLAXIS 3D and the HSsmall constitutive model to predict the lateral response of large scale piles in offshore clay conditions, reporting excellent agreement with the field tests. Overall, despite the expected changes in the soil state, several FE studies have demonstrated that the lateral response, especially in the small strain region, of impact driven piles in clay can

be reproduced with high accuracy by the current WIP modelling approach, provided that these models are properly calibrated.

Therefore this study focuses on installation effects in sandy soils, considering both conventionally impact driven piles and the most most promising technique reported in literature, vibratory driving. The common observation across various studies is that pile installation affects the surrounding soil state and consequently the lateral response of the piles. In detail, the two main phenomena that govern this behaviour is the change in void ratio; soil densification or loosening, and the redistribution of the horizontal stresses. The effect of pore pressure build up is typically found to be less significant [3], [20], [48] - especially for sand - that is usually sheared under drained conditions.

1.5.1 Effects of installation method on the soil state

Driven piles fall into the broader category of displacement piles; where as pushed into the ground they "displace" the surrounding soil and change the soil state around them. The extent of the affected zone around the pile is still not clear enough, with different studies reporting varying values [3], [25]. Therefore in this section an overview of the geomechanical response of the soil during installation is presented to set the basis for the numerical modelling.

Stress redistribution

Both impact and vibratory driving induce cyclic shearing in the adjacent soil leading to gradual contraction of the sand. As the volume of the adjacent soil decreases the horizontal confining stresses acting on the pile also tend to decrease [10], [29]; a phainomenon known as "friction fatigue" [28] or cyclic degradation [29]. It describes the realignment and loss of interlocking between grains, resulting in reduced shaft friction resistance f_s, with the lower limit being the residual resistance.

Measurements from the small-scale phase of the SIMOX project [20], the research of Stein [49] and Fischer [25], all focused on the installation effects in dense saturated sands, demonstrate that as the impact driven pile progresses towards a pressure sensor, radial stresses initially increase due to soil displacement. However, once the pile tip passes the sensor level, stresses gradually decrease due to the friction fatigue effect, as illustrated in Figure 1.4. According to Stein [49], this stress evolution distinguishes two different zones along the pile, one governed by the installation effect (installation induced stress increase) on the lower part of the pile and one governed by friction fatigue on the upper part of the pile, as shown in Figure 1.5.

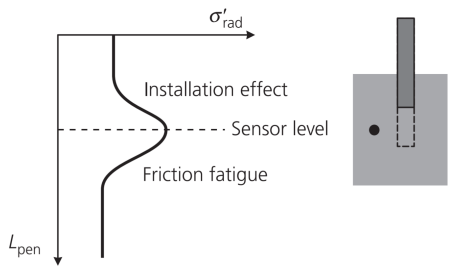

Figure 1.4: Development of radial soil stress during impact driving for a dense saturated sand, after [48]

While SIMOX relied on a single sensor located near the pile toe, the more comprehensive sensor array employed in Fischer [25] and Stein [48] provides a clearer picture of post-installation stress state in dense, overconsolidated, saturated sands at a radial distance of 0.33D across the embedment depth as illustrated in Figure 1.5, that shows an increase of installation induced stresses with depth. The increase at the upper, friction fatigue governed, part of the pile is limited while the pile toe region where the stress increase is significant is governed by the installation effect. A more accurate representation of the post-installation stress state is expected to improve predictions of lateral monopile behaviour.

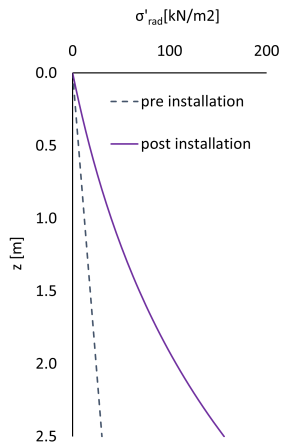

Figure 1.5: Post-installation effective horizontal stress state for an impact driven pile with a pile pentration depth (PPD) of 2.5m, after [48]

Interestingly, for vibratory driven piles horizontal stress changes are often negligible [20], [48] which may explain the better agreement of the WIP-based numerical models with field tests, as it will be discussed in the following chapters. Nonetheless, several studies report a localized increase in horizontal stresses near the pile tip for both vibratory and impact driven piles, though the effect is more pronounced for the latter [10], [23], [29].

Overall, a change in horizontal stresses in the surrounding soil due to pile installation will result in a change in the lateral response of the monopile. The strength and stiffness properties of the soil are dependent on the stress level, therefore increased horizontal stresses, in the case of impact driven monopiles will result in increased strength and stiffness properties of the soil and subsequently stiffer lateral response of the monopile under lateral loading. That is also reflected in the formulation of Hardening Soil constitutive models, where both strength and stiffness properties are stress dependent.

Void ratio changes

Achmus et al. [3] conducted large-scale field tests in dense to very dense sand, comparing pre- and post-installation CPTs at varying distances from the pile, to identify

changes in the soil state; specifically relative density, and ultimately discuss the effect of installation on the lateral response. In this study, Achmus explicitly attributes differences in load-bearing behaviour between impact- and vibratory-driven piles to the effects of installation on relative density. Loosening of the soil, indicated by a decrease in cone resistance, was observed up to a distance of 0.28D from the pile wall for both installation methods.However, the effect was notably smaller for the pile installed with reduced frequency and slower penetration rate (pile P1v), highlighting the influence of installation parameters. At a closer distance of 0.09D from the pile, dilation was still observed at the same or lower degree. The overall disturbance zone was found to extend up to approximately 0.46D. The effect is more pronounced for the vibro-installed monopiles except for the one with modified installation properties (slow installation). These findings align with observations by Hoffmann et al. [29] and reinforce the conclusion that void ratio changes, and consequently lateral response, are sensitive to installation frequency and duration.

Contrary to these observations, small-scale laboratory tests conducted during the SIMOX project [19], [20] reported densification around both hammered and vibrated piles installed in saturated medium dense and dense sands. Settlement measurements supported the presence of a densified "shell" approximately 0.15D inside and outside the pile wall. Similar findings are also reported by [48].

Further insights are provided by experiments from the University of Western Australia. Bienen et al. [10], using large-strain FE modelling validated against centrifuge tests in dense sand ($D_r = 68\%$), observed significant densification in the immediate vicinity of vibro-driven piles, and loosening at more distant zones. Fan et al. [23] confirms those observations with numerical modelling results for different relative densities from loose to dense sands (ranging from 38 to 88 %). Specifically, Fan et al. [23] reports densification regardless of the initial density for the hammered piles, both on the inside and outside of the piles, but more pronounced in the soil plug. Findings from the same study show that the sand tends to reach the same critical state void ratio regardless of the initial relative density, implying that densification is more pronounced in loose soils. The densification area extends horizontally to 2.72D in contrast to da Silva et al. [20]. Additionally significant decrease of the void ratio below the pile toe for every relative density was observed.

Pore pressure changes

As aforementioned the effect of pore pressure build up due to installation in the subsequent lateral response of monopiles is generally considered to be negligible, particularly in sandy soils. This is largely because piles are usually loaded laterally

after a sufficient time from installation has passed allowing for any excess pore pressure to dissipate [8]. Achmus et al. [3] mentions that post-installation CPTs showed that drainage occurred after 25 to 35 days post installation while Da Silva et al. [19] and da Silva et al. [20] observed rapid dissipation of excess pore pressure following both impact and vibratory installation in saturated dense sands. Similarly Stein [49] found no significant pore pressure build-up during both installation methods.

On the other hand, according to Hoffmann et al. [29] pore pressure build up may depend on the installation method. Minimal build-up was observed for impact driven piles -attributed to the long time between blows - while vibratory driving caused a transient increase in pore pressure, up to 1.6 and 1.4 times the initial values for non-cavitational and cavitational modes respectively. These so-called vibration modes are associated with the installation speed, where non-cavitational and cavitational corresponds to fast and slow driving respectively. However because dissipation time was not measured, it is unclear whether these changes affected the effective stress state at the time of lateral loading. It is mentioned that the pile installed with a non-cavitational mode (fast driving) exhibits the softer response while the impact driven pile was stiffer. That observation aligns well with the finding from Achmus et al. [3], namely that the negative effect of the vibratory installation was minimized on the piles installed with lower installation frequency and increased installation time.

According to Fischer [25], piles driven in unsaturated sand experience significantly greater grain rearrangement and effective horizontal stress increase compared to those driven in fully saturated conditions. This is attributed to reduced inter-particle shear transfer under saturated conditions due to transient pore pressure spikes, and lower frictional resistance. Consequently, fully saturated sand shows less pronounced dilative or contractive behaviour during pile driving, resulting in smaller net changes in effective stress. Notably, Fischer [25] reports that the horizontal stress measured near the pile tip at the end of installation can differ by more than a factor of two between unsaturated and fully saturated conditions, even in the same dense sandy soil.

Overview

Literature findings are generally diverse and sometimes contradictive regarding the effect of the installation method on the soil state and subsequently on the lateral response of monopiles. Nevertheless the conclusion that can be made is that vibratory driven piles generally exhibit softer response compared to hammered piles all else being equal, that pore pressure effects are transient and can have an effect on the subsequent lateral response, that the net radial stress increase post installation

is increasing with depth and that while void ratio effects changes may occur they are not considered decisive in determining lateral behaviour. Therefore it is assumed the the dominant - installation related - mechanism governing the lateral response of monopiles, is the change of effective horizontal stresses in the surrounding soil.

1.6 Numerical modelling of monopile installation

The common practice in FE modelling is to consider the pile as wished-in-place (WIP), thereby ignoring the effects of installation on the surrounding soil. Although this method offers computational efficiency and often yields relatively accurate results for the design of monopiles, several studies have shown that tends to underestimate the initial stiffness of monotonically laterally loaded monopiles [32], [35], [50] with potential implications on the predicted natural frequency of the supported structure. Incorporating installation effects into the FE model is expected to improve the accuracy of the foundation design and more realistically reflect in-situ conditions.

1.6.1 Explicit modelling - Large deformations methods

Several authors have attempted to explicitly model the installation procedure in the context of finite element modelling using the Coupled Eulerian-Lagrangian (CEL) approach [10], [23]. These models often validated against centrifuge tests offer valuable insights into how installation changes the soil state, as discussed earlier in Chapter 1. However, such methods remain computationally intensive and often underestimate the loading cycles required for the full penetration of the pile, compared to physical modelling. The underestimation of the lateral capacity is attributed to the significantly different number of loading cycles observed during physical and numerical modelling. Notably, Bienen et al. [10] reports 6000 “installation” cycles for physical modelling opposed to only 40 in numerical for the pile to reach the target penetration depth. Less cycles may lead to underpredict the changes in the soil state associated with the installation process, specifically friction fatigue, and therefore amplify the uncertainty in predicting the lateral capacity. Due to these limitations, this approach was considered unsuitable for the scope of this thesis.

1.6.2 Implicit modelling - Soil degradation zone

In response to the computational cost and complexity related to the aforementioned approach, there have recently been proposed simplified methods trying to capture

the installation effects on the soil rather than the installation procedure itself. In other words, the effect of the installation on the soil and consequently the lateral behaviour of the monopile is incorporated into the model by modifying the soil properties accordingly. Instead of modelling the installation procedure and subjecting the soil in cyclic loads that would consequently degrade its properties, in alignment with the friction fatigue concept, but also the loosening of the soil as reported by Achmus et al. [3], the pile is wished in place (WIP) for simplicity and the installation effect is directly assigned to the soil properties in a so-called degraded zone surrounding the pile, by means of correlating the post installation cone resistance curves to the constitutive model properties, that would have normally been affected by the installation. This method has been employed by several researchers [27], [34] and provides improved accuracy to the numerical model results. The modified soil properties can be obtained by means of empirical correlations of post-installation CPTs at the vicinity of the installed monopiles, and in the absence of such data for the majority of the newly executed offshore wind projects that method was considered not feasible. As an alternative, a modified version of this approach is adopted in this study, where the coefficient of lateral earth pressure is adjusted to reflect the increase in horizontal stresses due to installation, calibrated against analytically derived stress profiles, as will be discussed in detail later in this thesis.

1.6.3 Implicit modelling - Volumetric expansion zone

An approach is that of imposing volumetric strains to the adjacent soil as originally described by Tol and Broere [52] in an effort to incorporate into the model the volumetric expansion or compaction that has been noticed both in physical and numerical modelling. In other words, instead of modelling the procedure itself, the effect of it is assigned into the model; namely the soil is “artificially” expanded in order to mimic the stress increase that would have occurred during driving due to shearing in the pile-soil interface. This modelling technique; was used by Pisanò et al. [42] for piles installed in dense marine sand related to the PISA field test, improving the accuracy of the small strain stiffness of the pile under lateral loading. da Silva et al. [20] in an effort to capture the geomechanical effects on the soil during installation that were mentioned in Section 1.5.1 also introduced volumetric strains in a region, cluster around the pile, where the settlements were observed.

However it is important to mention that merely imposing isotropic volumetric strains cannot fully capture these anisotropic and non-uniform changes in soil fabric, structure, and stress orientation. The success of this method depends heavily on the calibration of volumetric strains to match known post-installation conditions. In re-

ality, different soil types (sand, clay, layered deposits) respond differently to pile penetration. A single prescribed strain field may not reflect key differences in soil response, leading to discrepancies when extrapolating to other sites, soils, or pile configurations and installation methods.

1.7 Conclusion and main findings

The main findings of the literature review, that will serve as the backbone of this thesis, can be summarized in the following points.

- The research focus should be on the small strains response of monopiles, that governs the dynamic behaviour of offshore wind turbines.
- Installation effects are significant only in sandy soils while the initial stiffness of laterally loaded monopiles in clay soils is very well predicted under the simplified WIP assumption.
- Pile installation results in changes in the soil state, most importantly relative density changes and stress redistribution in the vicinity of the pile. Pore pressure changes are generally found to be insignificant for sands.
- Installation effects are more pronounced in unsaturated dense sands, as the "transient undrained" response in saturated conditions limits these effects during pile driving.
- The post-installation effective horizontal stresses around the monopile, govern its lateral response. Void ratio changes are generally considered as less significant.
- A successful implementation of the installation effects into a FE model scheme, is expected to optimize the design of monopiles foundations for offshore wind turbines.
- The modelling approaches that show the greatest potential for engineering applications, are volumetric strains and a modified coefficient of lateral earth pressure, offering simplicity and the ability to capture the most important geomechanical effect, namely horizontal stress changes.

1.8 Research question

The literature study presented in this chapter leads to the following research question:

How to capture installation effects on the lateral response of monopiles within a generalized framework?

To address this main research question, the study is structured around two interlinked themes:

- The calibration of the soil constitutive model to model wished-in-place (WIP) response, and
- The modelling of installation effects, which modify the initial stress state around the monopile

1.9 Outline

This thesis project is organized in five main chapters. The current chapter provides the literature review, introducing the motivation and objectives of the study, discussing the effects of monopile installation on soil behaviour, and reviewing the numerical methods available to model their lateral response. The second chapter presents the FE model setup used throughout the project, including the mesh, boundary conditions, and material properties while also including the model validation. Chapter three outlines the calibration procedure that was followed to estimate the initial soil parameters and presents the results of the WIP models while chapter four describes the modelling approaches that were followed to capture installation effects for both impact- and vibratory-driven monopiles and presents the corresponding results from the enhanced models. Finally, chapter five summarizes the key findings and provides recommendations for practical implementation as well as suggestions for future research.

Chapter 2

Finite Element Model

2.1 Finite Element Model

The soil-structure interaction problem determining the lateral behaviour of a monopile under monotonic loading, is investigated by means of a FE model in PLAXIS 3D. The FE model is first validated against the results of Fazlighiyasabadi et al. [24] and Minga and Burd [37].

2.2 Model geometry and properties

Owing to the symmetry of the problem only half of the 3D geometry is modelled, with the vertical plane at y=0 being the plane of symmetry. The soil domain dimensions are decided as a function of the monopile dimensions such as to not affect the numerical results but also ensure reasonable computational time. The total model length in the loading direction is equal to 12 monopile outer diameters while the length in the perpendicular to the loading direction is equal to 4 diameters, as specified in [40]. The boundary conditions are defined such as to ensure symmetry with respect to the vertical planes, fixity at the lower boundary and free at the soil surface. An indicative model geometry is given in the following figure.

Regarding the pile geometry, the top is closed with rigid plate to allow for the force or prescribed displacement to be applied while the bottom of the pile remains open.

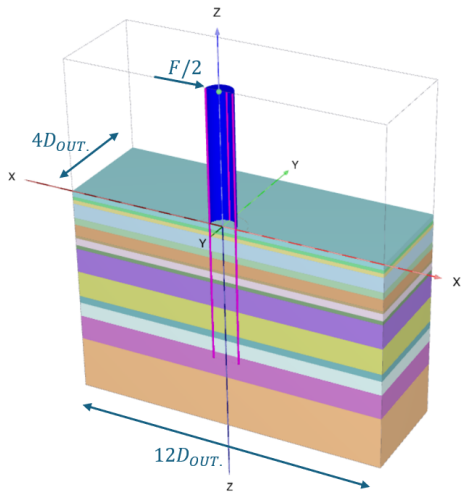

Figure 2.1: 3D finite element model indicative geometry

An overview of the main geometrical characteristics and installation methods of the piles studied are given in the Table 2.1.

Pile	Project	Installation	D [m]	PPD [m]	t [m]	e [m]
DM4	PISA [36]	Impact	0.76	3.98	0.014	9.98
DM7	PISA [36]	Impact	0.76	2.24	0.010	10.00
DL1	PISA [36]	Impact	2.00	10.61	0.038	9.90
P2h	VIBRO [3]	Impact	4.30	18.50	0.040	0.85
P1v	VIBRO [3]	Vibratory	4.30	18.20	0.040	1.00
6A-V	SIMOX [-]	Vibratory	–	–	–	–
8B-H	SIMOX [-]	Impact	–	–	–	–
Z10	Stein [48]	Impact	0.60	2.40	0.003	2.00

Table 2.1: Overview of pile characteristics (The geometrical characteristics of SIMOX piles are not included herein for confidentiality reasons).

2.3 Interface properties

To simulate the soil-pile interaction and allow for slippage (relative displacement), 12-node interface elements are added along the outer monopile surface. Their strength and stiffness properties are controlled by the reduction factor R_{inter} which correlates the interface properties to those of the adjacent soil cluster. Alternatively, a new separate material can be assigned to the interface elements allowing for custom properties independent of the adjacent soil. The first approach is generally followed throughout this thesis project, with the R_{inter} values summarized in the relevant Tables of Appendix A. For the validation of the model against Minga and Burd [37] and Fazlighiyasabadi et al. [24] the second approach was used; namely, a new material was assigned to the interfaces with the same stiffness properties but modified effective friction angle, denoted as ϕ'_{inter}, consistent with their original assumptions, as shown in Tables A.5 and A.9.

2.4 Mesh and calculation

Upon completion of the structure's modelling, the finite element mesh is generated whose quality directly affects the quality of the results but also the computational time. The governing elements being those at the shaft-soil interface. For that reason the coarse mesh refinement is selected for the soil surround the pile while a mesh refinement factor of 0.5 is assigned to the pile to better capture the interaction forces but also ensure reasonable computational cost. The results of a mesh convergence study conducted to decide on the adequate mesh quality are given in Appendix B.

Finite element calculations take place in sequential phases; the option of construction stages is used. A typical construction sequence for a laterally loaded pile, features the initial phase where the initial undisturbed soil stress state is calculated by means of a K0-procedure followed by the activation of the monopile geometry (pile plate and interface elements) in a single phase where the pile is introduced into the model as WIP. The application of the lateral loading at the pile top follows at the last stage.

2.5 Constitutive model

The choice of the soil constitutive model is of significant importance determining the stress - strain relationship and ultimately affecting the quality of the predictions. In

this study the focus is placed on the the pre-failure behaviour of the soil that governs the dynamic behaviour of offshore wind turbines that is related to the fatigue limit state (FLS), focused on small strains rather than ultimate capacity. The non-linear behaviour of soil even in the small strains region was first investigated by Burland [15] who employed local strain measurements in triaxial tests, unlike the conventional practice of using external measurements. These experiments revealed that the initial small strain shear modulus is nearly an order of magnitude higher than the secant shear modulus before yielding. Such behaviour cannot be captured by simple linear-elastic models and therefore implies the use of more advanced models capable of capture small strain nonlinearity and the increased stiffness of soil in that range of strains. The Hardening Soil model with small-strain stiffness (HSsmall) is considered the most appropriate for capturing the realistic behaviour of the soil in this strain range.

Considering the dynamic nature of the loading and the focus on the serviceability (SLS) and fatigue limit state (FLS), as well as the expected accuracy of predictions, the advanced constitutive models which predict the stress-strain relation more accurately than simple linear-elastic, perfectly plastic models as described above was chosen. Figure 2.2 illustrates the strain range that this study focused on considering the dynamic response and that justifies the use of this constitutive model.

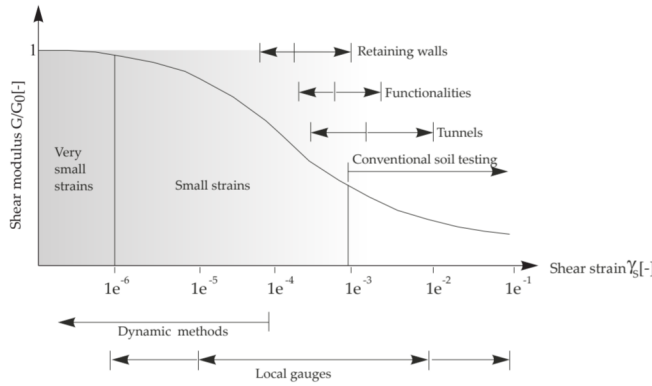

Figure 2.2: Strain dependency of shear stiffness with typical ranges from structures and laboratory tests (after PLAXIS Material Models Manual)

As aforementioned the adopted soil constitutive model is HSsmall. This model was selected because it can not only capture the hardening behaviour of soil under shear-

ing and compression but also accounts for the pressure-dependent stiffness through yield surface expansion. In contrast to the simple Hardening Soil model, HSsmall can also capture small strain non-linearity and irreversibility thus avoiding overestimation of displacements. The two fundamental features of HSsmall is the stress dependency of the stiffness even in the small strain region controlled by G_0 and the small strain non-linearity controlled by $\gamma_{0.7}$. These two additional parameters enable HSsmall to more accurately capture monopile response in the small-strain region, which is critical in this study since the focus is on initial stiffness governing the dynamic response of offshore wind turbines. However, it is important to mention the inherent limitation of this constitutive model; namely the fact that it cannot capture the softening behaviour of soils, particularly relevant for dense sands. Nevertheless, since the main focus in on small strains and initial stiffness, the potential implications of this limitation; namely overprediction of the ultimate capacity were considered to be of little importance and therefore were neglected in this study.

A brief description of the main parameters that define the mechanical behaviour of the soil when using this constitutive model is also given in the section. The Hardening Soil models feature stress dependency, expressed through three different confining stress-dependent moduli; namely E_{50}, E_{oed}, E_{ur}. The secant modulus E_{50} which corresponds to 50% of the value of the maximum shear deviatoric stress q_f is dependent on the minor principal stress and is given by the following formula.

$$E_{50} = E_{50}^{ref}(\frac{ccos\phi - \sigma_3' sin\phi}{ccos\phi + p_{ref} sin\phi})^m \tag{2.1}$$

E_{ur} on the other hand defines the slope of the unloading-reloading part of the stress-strain curve in a triaxial test and is given by the following formula.

$$E_{ur} = E_{ur}^{ref}(\frac{ccos\phi - \sigma_3' sin\phi}{ccos\phi + p_{ref} sin\phi})^m \tag{2.2}$$

At last E_{oed} gives the tangent stiffness for primary oedometer (one-dimensional compression) loading. Note that the stress dependency level is controlled by parameter m and that in the HSsmall formulation effective stresses σ' are negative in compression. The stiffness parameters in the context of a triaxial test are illustrated in the following figure.

These were the common parameters of Hardening Soil and Hardening Soil with Small Strains models. The distinct characteristic of HSsmall is in the small-strains,

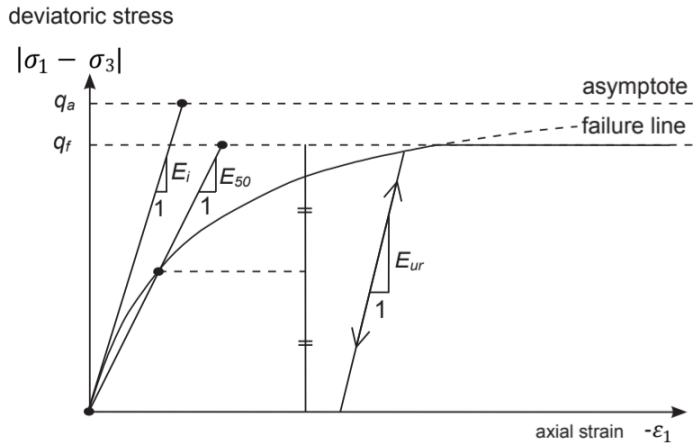

Figure 2.3: Stiffness parameters $E_i = E_0$, E_{50} and E_{ur} in a triaxial test (after PLAXIS Material Models Manual)

as its name implies, and is controlled by the small-strain shear modulus; G_0, and the threshold shear strain; $\gamma_{0.7}$ given by the following formulas.

$$G_0 = G_0^{ref}(\frac{ccos\phi - \sigma_3' sin\phi}{ccos\phi + p_{ref} sin\phi})^m \tag{2.3}$$

$$\gamma_{0.7} = \frac{1}{9G_0}[2c'(1 + cos2\phi' - \sigma_1'(1 + K_0)sin2\phi'] \tag{2.4}$$

In contrast to the more complex formulation of the stiffness properties, the strength of the soil in this model is constant - not stress dependent - and is described by the effective friction ϕ' and dilation ψ angles and cohesion, c. Lastly, an overview of the key model parameters is given in Table 2.2.

Parameters	Description	Unit
E_{50}^{ref}	Secant stiffness modulus	kPa
$E_{\text{oed}}^{\text{ref}}$	Oedometer stiffness modulus	kPa
$E_{\text{ur}}^{\text{ref}}$	Unloading-reloading stiffness modulus	kPa
G_0^{ref}	Small strains shear modulus ($\varepsilon < 10^{-6}$)	kPa
ν_{ur}	Unloading-reloading Poisson's ratio	–
$\gamma_{0.7}$	Threshold shear strain at $G/G_0 = 0.722$	–
R_f	Failure ratio	–
m	Power for stress-level dependency of stiffness	–
c	Cohesion	kPa
φ	Angle of internal friction	degree
ψ	Dilatancy angle	degree

Table 2.2: Overview of HSsmall model parameters

2.6 Validation

The validity of the numerical models that were used in this study is verified against the large-scale field tests of PISA [14] and VIBRO-Cuxhaven [3], both investigating the lateral bearing capacity of large diameter, impact and vibratory driven, monopiles in predominantly dense, partly saturated sandy soils. Validation is performed against the results of piles DL1 (PISA) and P2h (VIBRO-Cuxhaven) by comparing the obtained horizontal reaction force (H) versus mean lateral displacement at the mudline level (ν_g) against those reported in previous finite element (FE) studies by Minga and Burd [37] and Fazlighiyasabadi et al. [24]. In the PISA project, the original load-displacement curves, are originally reported at the mudline level [36], [50], whereas for the VIBRO-Cuxhaven test, the displacements were recorded at varying heights above the mudline Achmus et al. [3]. For consistency and cross-project comparison, the Cuxhaven displacements were transferred to the mudline level, using the deformed shape given in Gattermann et al. [26]. The geometrical characteristics for the aforementioned piles are summarized in Table 2.1. The relevant soil properties are summarized in Appendix A.

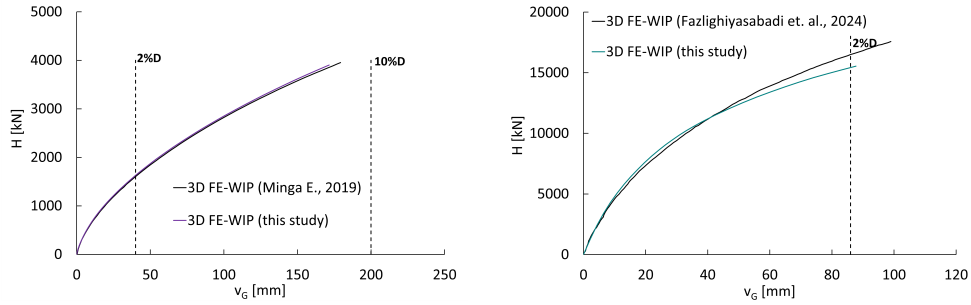

Figure 2.4: Comparison of the lateral response between the results of the present FE models and previous numerical studies. Left: PISA pile DL1 (Minga and Burd [37]). Right: VIBRO-Cuxhaven pile P2h (Fazlighiyasabadi et al. [24])

The developed FE models show very good agreement with the published results, and prove that the present WIP modelling approach can adequately capture the lateral response of a monopile under monotonic loading. In both cases, the goal was to replicate the authors' numerical results using their original constitutive model parameters, as summarized in Tables A.5 and A.9. For the model of the VIBRO-Cuxhaven pile, it is important to mention that the stiffness properties of the clay-till layers were not explicitly provided in Fazlighiyasabadi et al. [24]. Instead, representative values were estimated using empirical correlations from DNV-GL-ST0126 [22], as described in Appendix A. That is expected to be the main source of any minor deviation between the models.

In the validation models, the relative displacement of the pile toe to the the outer soil was modelled via an interface at the tip, while the weight of the pile was neglected, to align with the original models. For the models following in this study, the pile weight is considered for a more realistic representation while the interface at the pile toe was neglected to optimize the calculation time. This modelling choice is supported by the observation that the pile toe has a negligible effect on the overall response, as demonstrated in the sensitivity analysis provided in Appendix C.

Chapter 3

WIP response modelling

Establishing a method to obtain constitutive model parameters based on in-situ data is fundamental for predicting the lateral response of monopiles, since this controls the WIP response of a pile, and defines the optimization margin by incorporating installation effects into the model. The comparison of the WIP response of the same monopile based on different approaches showcases the need for an initial soil parameters interpretation scheme. It is evident that different approaches for estimating the constitutive model parameters lead to different level of agreement with the field test and consequently different degree of underestimation and level of required volumetric strain. In other words, it is the initial soil conditions that not only define the WIP response but also determine the calibration of the installation parameter.

The proposed approach is to first interpret the soil properties and calibrate the initial constitutive model parameters. After the accuracy of the model is further improved by incorporating the installation effect in the FE model. Hence, it has been decided that PLAXIS 3D and HSsmall, a widely used constitutive model in industry that captures small-strain plasticity, can capture soil hardening, and offers a balance of accuracy and complexity, will be used. This chapter aims to describe the basic features of HSsmall, its adequacy for this problem, possible limitations and their implications.

3.1 Methodology

The present section aims to describe the interpretation methodology - calibration of the initial soil parameters - followed throughout this study based on results obtained by in-situ testing and through empirical correlations.

In literature there is a number of different approaches to calibrate those constitutive model parameters: either entirely against CPT data as in Brinkgreve et al. [13], or using a combination of in-situ and laboratory test data as in Minga and Burd [37] and Zdravkovic et al. [57]. In the present study the second approach with some modifications is followed.

To evaluate the effectiveness of each method, a comparison is conducted for the PISA-DM4 pile on the basis of the prediction accuracy of the load displacement curve. The assessment focuses on lateral displacements at the mudline up to 2%D. In general, the SLS is defined as a rotation of 0.25 degrees at the mudline [22] which for the slenderness ratios (PPD/D) and pivot depth characteristic of rigid monopiles used in offshore wind corresponds to a lateral displacement of about 2%D. Project experience indicates that FLS deflection levels remain well below this threshold, while a lateral displacement of 10%D is typically considered the ULS limit. Field data for the PISA test campaign are reported by [36], and the pile's geometric characteristics are listed in Table 2.1. The comparison depicted in Figure 3.1, shows that the correlation by Brinkgreve et al. [13] significantly underestimates the lateral response, in alignment with [16]. In contrast, both the correlations by Minga and Burd [37] and the approach proposed in this study both result in comparably good agreement, with the latter yielding slightly softer responses. Nevertheless, it is evident that all three different methodologies underestimate the stiffness and lead to different response. A similar pattern, wide spread of the prediction accuracy across different methods and a general tendency to underpredict the initial stiffness, is reported by Machaček et al. [35] for a blind prediction contest on laterally loaded impact driven piles in dense sand, despite the availability of detailed input data. These findings highlight the importance of initial constitutive model parameter calibration and the need to establish a robust methodology to capture the WIP response.

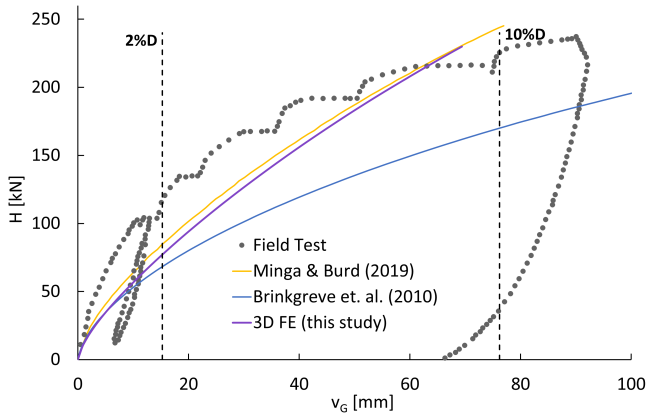

Figure 3.1: Comparison of different correlations for the calibration of the initial soil parameters in terms of accuracy in predicting the lateral load behaviour of the PISA-DM4 pile [36].

Based on the previous comparison and the lack of justification for the non-degrading with strain stiffness properties used by Minga and Burd [37], as well as the simplified approach of Brinkgreve et al. [13], which relies solely on the relative density D_r; this study adopts a new calibration workflow. The constitutive model properties for each soil layer corresponding the three different models presented in Figure 3.1 are summarized in Tables A.5, A.6 and A.7.

In this study, the strength parameters, effective friction ϕ' and dilation angle ψ, are derived based on the relative density (D_r) of the soil, following the empirical correlation by Schmertmann [45]. The relative density is correlated to the cone resistance curve according to Baldi et al. [7] and therefore potential inaccuracies related to disturbance of reconstituted sand samples in triaxial or direct simple shear testing are avoided. Note that the dilation angle, ψ is obtained as a function of, the CPT derived, effective friction angle through the following formula: $\psi = \phi - 30$. Lastly, in order to avoid numerical instabilities, the cohesion for sand layers, c, was set equal to 0.1 kPa unless stated otherwise.

In line with the formulation of the constitutive model, and consistent with this study's interpretation scheme, the small strain shear modulus G_0 is considered the key parameter governing initial stiffness and therefore its calibration is essential for the quality of the prediction. Its value is typically obtained from SCPT measurements

through empirical correlations proposed by Robertson [44] or Seed and Idriss [46] the value of G_0 is determined. Depending on the availability of data G_0 can also be estimated based on dilatometer testing, as follows:

$$G_0 = \rho V_s^2 \tag{3.1}$$

The different Young moduli are subsequently derived as a function of G_0 as described in the PLAXIS reference manual [9]. Specifically, the initial Young's modulus, E_0, is related to G_0 through Hooke's law as follows:

$$E_0 = 2G_0(1+\nu) \tag{3.2}$$

The unloading-reloading modulus E_{ur} follows from a modified version of Alpan's diagram [5] while E_{50} is derived according to the following equation, according to PLAXIS reference manual [9]:

$$E_{50} = E_{ur}/3 \tag{3.3}$$

At last, E_{oed} is assumed to be equal to E_{50} unless otherwise stated. A schematic overview of the entire calibration workflow is shown in the following Figure.

$$CPT \xrightarrow{Baldi} D_r \xrightarrow{Schmertzmann} \text{strength } (\varphi, \psi)$$

$$(S)CPT \xrightarrow[Seed\&Idriss]{Robertson\ or} G_0 \xrightarrow{\nu} E_0 \xrightarrow{mod.\ Alpan} E_{ur} \rightarrow E_{50}, E_{oed}$$

Figure 3.2: Proposed constitutive model properties interpretation scheme

A full list of the numerical values for the constitutive model parameters per soil layer for every simulation presented in this study is given in Appendix A.

It is important to highlight the effect of the overconsolidation ratio (OCR) and the resulting coefficient of lateral earth pressure at rest, K_0 -which together reflect the history of the soil- on the lateral behaviour of monopiles. However, their interpretation often involves considerable uncertainty; since detailed soil history is not always available. The OCR and K_0 are defined as follows:

$$OCR = \frac{\sigma'_p}{\sigma'_\nu} \tag{3.4}$$

$$K_0 = \frac{\sigma'_h}{\sigma'_\nu} \tag{3.5}$$

where σ'_p is the preconsolidation stress, σ'_ν is the current vertical effective stress, and σ'_h is the horizontal effective stress. An alternative way to define overconsolidation in PLAXIS is through the Pre-Overburden Pressure (POP) given by the following Equation:

$$POP = \sigma'_p - \sigma'_\nu \tag{3.6}$$

In this study the Pre-Overburden Pressure (POP) or Pre-Overconsolidation Pressure (POP) is first decided to calculate the OCR for overconsolidated (OC) layers, as follows:

$$OCR = \frac{POP + \sigma'_\nu}{\sigma'_\nu} \tag{3.7}$$

The uncertainty stems from estimating the preconsolidation stress, which depends on the availability and quality of historical information about the history of the soil, such as previous excavation records, as in the case of the Cuxhaven field test [43], or geological events (e.g. glacial loading). When limited data are available, the decision may be partly based on engineering judgement. To evaluate the effect of this uncertainty on the lateral response, a sensitivity study was conducted, as described in Appendix A, to asses how different OCR assumptions affect the lateral response.

An increased OCR leads to a higher K_0, which consequently increases the horizontal stresses around the pile and ultimately the stiffness parameters of the soil; namely E_{50}, E_{ur}, and G_0, as described in equations 2.1, 2.2, 3.1 and 3.2. The formulas used to calculate K_0 under normally consolidated and overconsolidated conditions are:

$$K_0^{NC} = 1 - sin\phi' \tag{3.8}$$

$$K_0 = K_0^{NC} OCR^{sin\phi'} \tag{3.9}$$

where K_0^{NC} corresponds to normally consolidated conditions and K_0 corresponds to overconsolidated soils.

3.2 Results

The accuracy of the prediction when modelling the pile as WIP strongly depends on the correlations used to derive the constitutive model parameters and consequently determines the optimization margin, as clearly illustrated in Figure 3.1. Through the interpretation methodology that was described in the previous section the initial constitutive model parameters were derived, as summarized in Appendix A, Tables A.7, A.10, A.11 and A.14. These findings indicate that the accuracy of the WIP model is dependent on the installation method. They highlight the need to incorporate installation effects when modelling impact driven piles while demonstrating the WIP model's adequacy for vibratory driven monopiles. This conclusion is supported by the findings of literature review; pressure measurements from [20], [48], [49] confirm the minimal increase in horizontal stresses and lateral displacement associated with vibratory driving in contrast to the the increased post-installation stresses observed for impact driving.

3.2.1 Impact driven piles

The underestimation of the initial secant stiffness at a displacement level of $2\%D$ at mudline level is consistently observed for the impact driven piles in PISA [36], SIMOX [19], [35] and in the tests reported by [48], as shown in Figure 3.3. In contrast, the WIP model unexpectedly overestimates the response for the impact-driven pile investigated in the VIBRO-Cuxhaven field test [3]. The load-displacement curves in Figure 3.3 highlight varying levels of prediction accuracy among the different piles, nevertheless all models, with the exception of the Cuxhaven pile, underestimate the initial stiffness.

A closer inspection of each field test and its corresponding load-displacement curve can help identify the underlying mechanisms responsible for the observed differences in the WIP model accuracy. Specifically, the FE models for piles DM4 and DM7 exhibit the softest responses, underestimating the secant stiffness at a displacement equal to $2\%D$ at the mudline level by 60% and 40%, respectively while pile DL1 shows a much smaller underestimation of around 13%. As described in Appendix A and B, piles DM4 and DM7 are installed entirely above the water table (i.e., in unsaturated conditions) while pile DL1 is partially in saturated and partially

in unsaturated conditions. According to [25] - as discussed in Chapter 1 - installation effects are more pronounced in unsaturated conditions, which may explain the greater degree of underestimation for these piles. In other words, the soil around piles DM4 and DM7 likely underwent more intense dilation, resulting in increased resistance and more significant installation effects, which the WIP model fails to accurately capture. However, since saturated conditions are the representative for offshore environments and therefore more relevant to the scope of this thesis, pile DL1 is considered the reference case for the PISA project in this context.

On the contrary, for the impact driven pile P2h from the VIBRO-Cuxhaven project [3], the WIP model overestimates the response. Fazlighiyasabadi et al. [24], Blok [12] and Gavin et al. [27] confirm these findings using the same FE program and constitutive model (PLAXIS 3D - HSsmall). These studies attribute the discrepancy to the inability of the constitutive model to capture softening effects in dense sands or the lack of creep modelling. These findings could also be explained by comparing the relative density, D_r, between the different projects. As illustrated in Figure 3.4 the Cuxhaven sand is less dense compared to PISA, SIMOX and Stein [48]. This indicated reduced dilation during installation and consequently limited stress increase. Therefore the WIP model does not underestimate the stiffness of this pile unlike in the other cases. That argument is further supported by Achmus et al. [3] who reported decreased cone resistance in the post-installation CPTs performed around the monopiles at a distance of 0.4 and 1.2 m. While the alternative interpretation scheme proposed by Fazlighiyasabadi et al. [24], also based on overconsolidated soil conditions, yields better agreement compared to the proposed in this study approach it is not adopted herein. The improved agreement is likely attributed to the use of site-specific correlations for the Cuxhaven site, which could limit the robustness of the approach. To maintain consistency across all case studies, the same interpretation methodology is applied to Cuxhaven. It is worth mentioning that an alternative interpretation of the Cuxhaven sand as normally consolidated was also explored, as presented in Appendix A, with the corresponding properties listed in Table A.13. This interpretation yielded a response more consistent with the general trend observed across the remaining tests, where WIP models tend to underestimate the stiffness of impact-driven monopiles.

The results of the WIP model for pile Z10 studied by Stein [48] in dense overconsolidated and fully saturated sand, focused in very small strains, approximately $0.4\%D$ at the mudline level, indicate that the response is underestimated as well. At last, similar level of underestimation is observed for the impact driven SIMOX-8B-H pile. Despite the presence of a clay layer, the profile up to a depth of $z = 1D$, consists of very dense sand which seems to control the lateral behaviour of the pile and deter-

mine installation effects. Overall the accuracy of the FE model WIP predictions, as presented in this Chapter, highlights the need to incorporate installation effects into the FE model.

It should be noted that all horizontal displacements refer to the mudline level, except for pile Z10, where the displacement denoted as v_t^*, is reported at a height of 0.6 m above the mudline due to limitations in the available data. The displacements are normalized by the outer diameter of the pile, according to the following expression:

$$v^* = \frac{v}{D} \tag{3.10}$$

For pile 8B-H of SIMOX, the horizontal load is also normalized to preserve confidentiality:

$$H^* = \frac{H}{LD^2\gamma'} \tag{3.11}$$

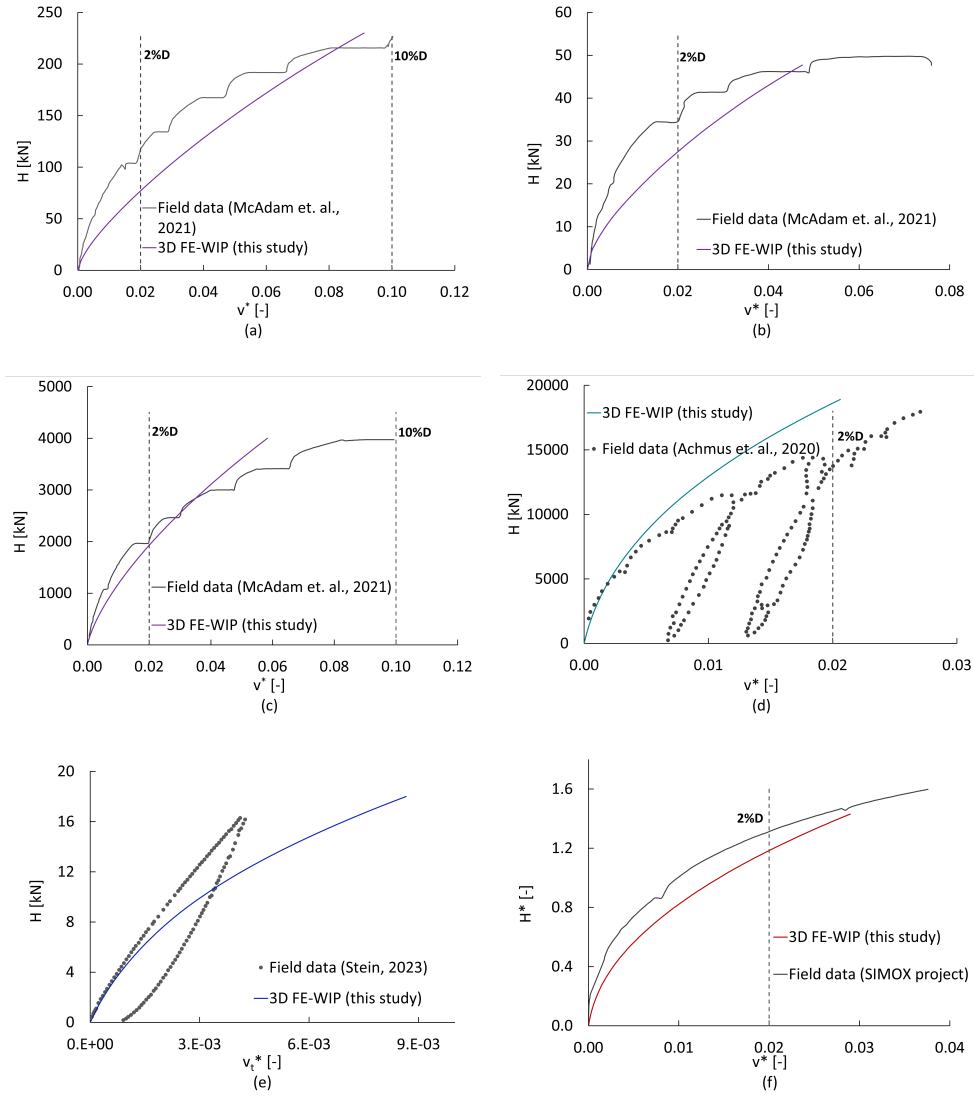

Figure 3.3: Lateral response of impact-driven monopiles. Comparison between field measurements and 3D FE-WIP simulations for piles: (a) PISA-DM4, (b) PISA-DM7, (c) PISA-DL1, (d) Cuxhaven-P2h, (e) Stein-Z10, and (f) SIMOX-8B-H.

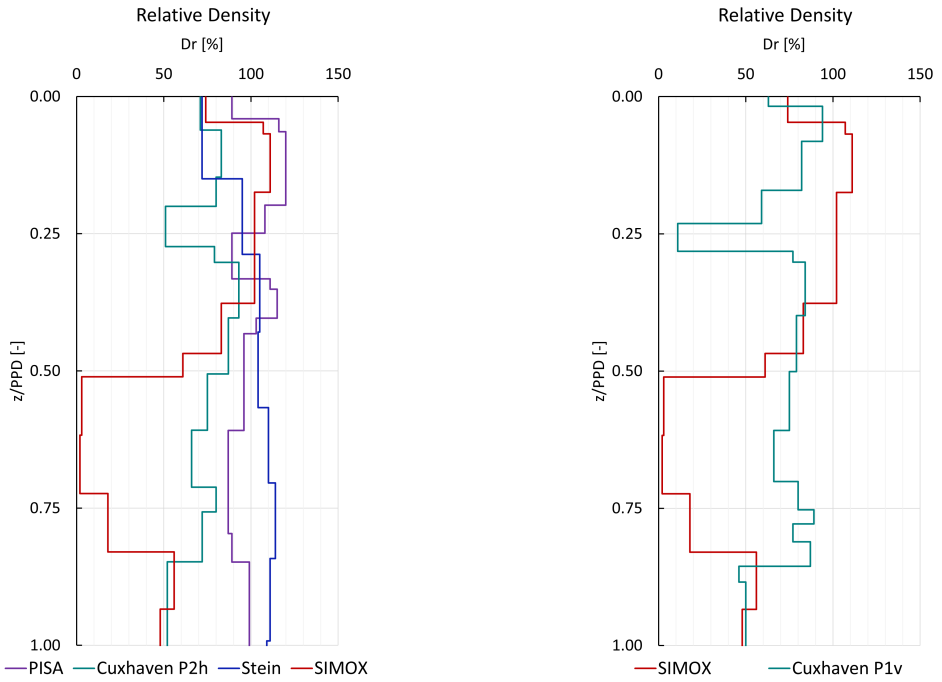

Figure 3.4: Comparison of relative density profiles normalized with respect to pile penetration depth (PPD) for the impact-driven (left) and vibratory-driven (right) monopiles.

3.2.2 Vibratory driven piles

The WIP FE model predicts the response of vibratory-driven piles studied in the SIMOX tests with good accuracy, while it overestimates the response of the VIBRO-Cuxhaven piles [3], as shown in Figure 3.5. That aligns well with the findings of [3] who reports reduced cone resistance in post-installation CPTs suggesting degraded soil properties. Also considering the fact that usually no horizontal stress increase is observed for vibratory driven piles [48], [49], [20], as discussed in Chapter 1, the WIP assumption is plausible for vibratory driven piles. It should be noted that for the VIBRO-Cuxhaven tests, the comparison of the modelled and measured field response is performed in terms of uncorrected load displacement curves, as indicated by [3]. Since the numerical model in this study explicitly includes the localized soil stratig-

raphy, CPT-based stiffness parameters, and pile geometry and loading characteristics for each test location, comparison with the uncorrected curves ensures consistency in the evaluation.

To further investigate the overprediction observed for pile P1v, an alternative interpretation assuming normally consolidated soil conditions was developed. This adjusted set of constitutive model parameters, summarized in Table A.12, led to significantly improved agreement with the field test, as described in Appendix A. These results can support the previous finding that WIP models are generally adequate for vibratory-driven piles while also highlighting the uncertainty associated with the stress state in Cuxhaven.

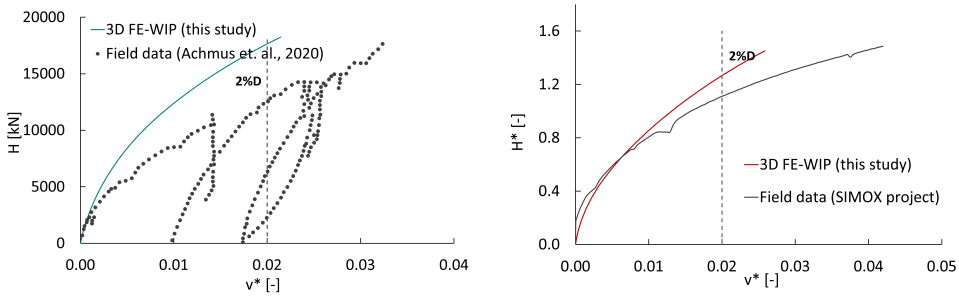

Figure 3.5: Lateral response of the vibratory driven monopiles. Comparison between field measurements and 3D FE-WIP simulations for piles: Cuxhaven-P1v (left) and SIMOX-6A-V (right)

Chapter 4

Implicit modelling of installation effects

This chapter presents the calibration of the installation parameters, namely the volumetric strain ϵ_{vol}, and the modified coefficient of lateral earth pressure at rest, $K_{0,mod}$. The calibration is carried out against the global response of the monopile, using three different field tests; PISA [50], TU Braunschweig-Stein [48] and SIMOX, to ensure applicability across varying soil stratigraphies and pile geometries. The ability of the volumetric strain to produce realistic post installation stress profiles is verified against an analytical expression, ensuring that the governing factor for the lateral pile behaviour; namely the post installation horizontal stress state, is realistically reproduced. In the second part of this chapter, an alternative approach including the modification of the lateral earth pressure coefficient, K_0, is presented. As a result, the models with the installation effect included yield increased stiffness and improved agreement with field observations, as discussed in section 4.2.

4.1 Methodology

4.1.1 Volumetric strain

The approach of Tol and Broere [52] and Pisanò et al. [42] is followed in this study, chosen for its simplicity making it a reliable and easy to use tool for engineering ap-

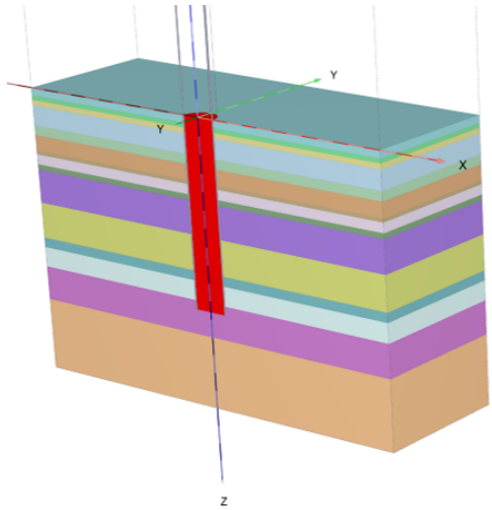

Figure 4.1: Soil plug (red coloured volume) where the installation effect ϵ_{vol} is applied

plications. The implementation of this method in the FE environment of PLAXIS 3D is presented in this paragraph aiming to give a detailed description of the necessary steps involved in that process. As extensively described in Chapter 1, the installation of monopiles in dense sandy soils will increase the horizontal confining stresses, depending on the installation method, resulting in increased initial stiffness. The effect of the installation on the stress state can be artificially incorporated in the model by imposing positive planar volumetric strain; expansion of the entire soil plug as illustrated in Figure 4.1. In the case of stratified soil profiles, the volumetric strain is applied exclusively to the dense sand layers, since only those are expected to dilate during driving. A uniform volumetric strain is applied, and is calibrated in terms of global response for the different piles examined, in an effort to make this method practical yet accurate for predicting the lateral response of monopiles. Following the initialization of the geostatic stresses, the soil inside the pile is expanded prior to the WIP phase, to account for the displacement and dilation of the soil that would typically occur when a monopile is impact driven into the ground.

Then the pile geometry and interfaces are activated while the displacements and small-strains are reset to zero. In this way the strain history is disregarded and the calculation of this phase starts from a zero-displacement field. Nonetheless, the effect, increased horizontal stresses and therefore increased stiffness, is passed on

through the state parameter. The HSsmall model captures this stress-dependency by modifying stiffness moduli as a function of the mean effective stress, as described by the following generic formulation:

$$E = E_{ref}(\frac{p}{p_{ref}})^m \tag{4.1}$$

It is evident through the previous expression, that the imposed volumetric strain increases the horizontal and mean effective stress (p) around the pile, as illustrated in Figure 4.2, resulting to a corresponding increase in stiffness. This ultimately results in a stiffer overall response of the monopile. For clarity the sequence of the calculation phases is given as follows:

- Initialization of stresses using the K_0-procedure
- Application of the volumetric strain (ϵ_{vol}) in the soil plug
- Activation of structural elements and interfaces (WIP phase) while resetting displacements and small strains
- Application of the static load or prescribed displacement at the pile's head

Figure 4.2 illustrates the effective horizontal stress field after activation of the volumetric strain for pile DL1 of the PISA project. It is clear that the soil expands and the horizontal stresses around the pile increase with depth. Although a uniform volumetric strain is applied within the soil plug, the resulting stress increment is greater at depth due to the higher confinement, which resists the expansion more strongly and thus translates the same strain into higher horizontal stresses. It is also clear from Figure 4.2 that the stress increase is more pronounced in the vicinity of the pile, and decreases with the distance from the pile, accurately reproducing what has been reported by several researchers [3], [25], [48].

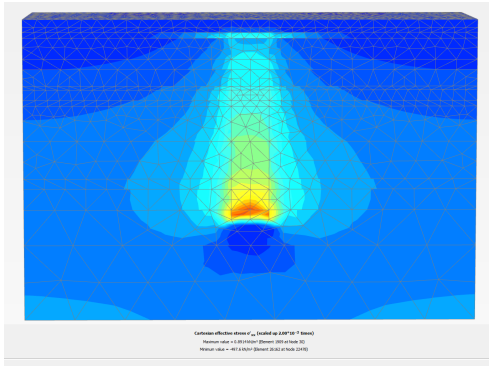

Figure 4.2: Effective horizontal stress field for pile DL1 after application of a planar volumetric strain equal to 1% (obtained by PLAXIS 3D)

Note that the installation parameter is applied only to the impact driven monopiles based on the findings of the literature review and the WIP modelling that were presented in Chapters 1 and 3 respectively.

The post-installation effective horizontal stress state, as predicted by the analytical expression 4.2, proposed by Stein [48], is used in this study as a benchmark to verify that the stress state resulting from ϵ_{vol}, remains realistic.

$$\sigma'_{\text{h, post}}(PPD, z) = \sigma'_{\text{h,pre}}(z) \cdot \left[1 + \left(\frac{1}{\beta} - 1\right) \cdot e^{-\alpha(PPD-z)}\right] \tag{4.2}$$

In this expression, the post installation stress state is expressed as a function of the initial horizontal effective stress ($\sigma'_{\text{h,pre}}(z)$), the pile penetration depth (PPD) and a set of two dimensionless parameters; the soil stress amplification factor (β), controlling the magnitude of soil stress increase due to pile installation, and the exponential decay factor (α), which captures the reduction of this effect with depth due to friction fatigue, as discussed in Section 1.5.1. The decay factor (α) is defined following Alm and Hamre [4] due to its practical direct correlation with CPT data, as follows:

$$\alpha = \frac{\sqrt{q_c/\sigma'_\nu}}{80} \tag{4.3}$$

The stress amplification factor β is defined according to Fischer [25] for sands of different densities. For clay layers and loose sands a value of β equal to 1 is proposed in the present study, reflecting no horizontal stress increase due to dilation during pile driving. The density dependent β values are summarized in Table 4.1. The values of the α and β parameters used per soil layer for the piles investigated in this study, are summarized in Tables C.1, C.2 and C.3 . For consistency and to align with the soil interpretation that was used in this study (Table A.14) the post installation stress state is calculated at the middle of each layer, for enhanced accuracy opposing to the approach of Stein [48] that assumes a uniform soil properties across the entire depth and therefore uses a single average value of the parameters.

	Loose & Clay	**Medium dense**	**Dense**	**Very Dense**
D_r [%]	0–30	30–70	70–100	100–120
β [-]	1.00	0.60	0.20	0.15

Table 4.1: Classification of soil relative density ranges and corresponding β values for saturated conditions.

The post-installation stress profile derived from the analytical expression of Stein [48] using the aforementioned calibrated parameters, based on pressure measurements at a scaled radial distance of $0.33D$ from the pile's wall, serves as a reference to verify that the stress profile obtained by imposing the volumetric strain parameter remains realistic and to calibrate the $K_{0,mod}$ as explained in the following section. It should be noted, however, that this analytical expression has inherent limitations. The correlation between the stress amplification factor β and the relative density D_r is defined as a stepwise function rather than a continuous closed-form equation. As a result, small variations of D_r around the density thresholds may lead to significantly different stress amplification values, and therefore different post-installation stress states. Moreover, since β is directly dependent on D_r, the predicted post-installation stress state can vary for the same soil depending on the D_r correlation used, as different correlations may yield different relative density values. To ensure consistency, the D_r values used for the stress profiles in the following sections are interpreted using the same correlation as outlined in Section 3.1.

4.1.2 Modified coefficient of earth pressure at rest

The installation parameter that has been presented so far, namely a planar volumetric strain on the entire soil plug, effectively manages to replicate the increased

post-installation stress state not only resulting in an increase of the radial stresses with depth but also ensuring a decaying effect with the distance from the pile in line with experimental [3], [25], [48] and numerical [23] findings. However, an alternative approach is presented in this chapter to replicate the increase in effective horizontal stresses due to pile driving and accurately capture the subsequent lateral response under monotonic loading. That involves modifying accordingly the coefficient of earth pressure at rest, K_0, while the pile is conventionally modelled as WIP, to match the stress state resulting from Equation 4.2. It is important to mention at this point that only the K_0 is modified to reflect the increase in horizontal stresses and not the overconsolidation ratio. The post-installation coefficient, $K_{0,mod}$ is defined as follows:

$$K_{0,mod} = \frac{\sigma'_{h,post}}{\gamma' z} \tag{4.4}$$

Although it is clear that modifying the K_0 applies a uniform change across the entire soil layer, as summarized in Tables C.1 and C.2, this simplification inaccurately implies that installation affects the entire soil domain equally by increasing the effective horizontal stresses to the same extent. However, it is believed that for small strains; where a limited part of the soil is mobilized, this will result in improved agreement with the field test. For larger displacements, equal to 0.1D at the mudline level, this method is expected to overestimate the stiffness since a greater - unrealistically stiff part of the soil domain - will be mobilized. Nevertheless, for the purposes of this study, this approach is believed to be adequate given its reduced complexity, practicality for engineering design, and ability to improve agreement with the observed lateral response.

4.2 Calibration

As previously mentioned, a calibration exercise of ϵ_{vol} is first performed on the basis of global response of the impact driven monopiles in partly and fully saturated conditions, namely piles PISA-DL1 [50], SIMOX-8B-H and Stein-Z10 [48] respectively. The resulting values are considered as site specific calibrated. The results indicate that an ϵ_{vol} equal to 1 $\%$ is required for an improved agreement with the field tests response, as illustrated in Figure 4.3. On the contrary the response of vibratory driven piles is already very well captured by the simple WIP model, without considering installation effects. That as also mentioned in Chapter 3 aligns well with the findings of [48] and [20], concluding that the post-installation horizontal

stress state is hardly affected by vibratory driving, and therefore the initial soil state parameters are considered representative of the post-installation stress state.

Despite differences in pile diameters, penetration depth and soil properties all piles examined in this study exhibit similar PPD/D ratios, indicating comparable response. Moreover, they are are embedded in predominantly dense sand, which is expected to dilate under shearing during installation and consequently increase the confining pressure and stiffness under monotonic lateral loading. Therefore an $\epsilon_{vol} = 1\%$ consistently improves the agreement for all cases and may serve as a practical starting point for future projects involving impact driven monopiles in similar soil conditions.

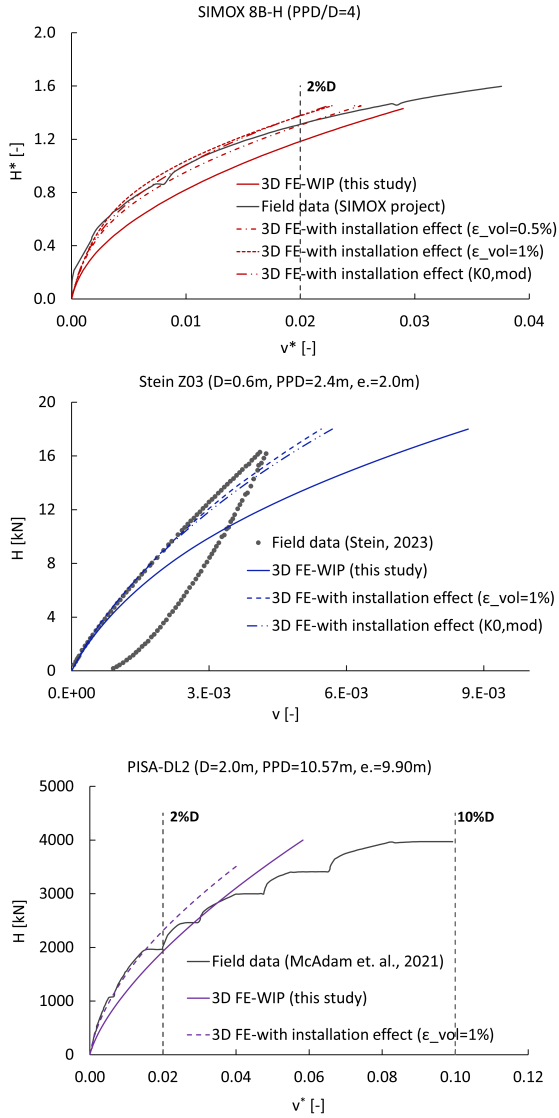

Figure 4.3: Lateral response of impact driven monopiles SIMOX-8B-H (top), Stein-Z10 (middle) and PISA-DL1 (bottom) with installation effect.

To verify that the stress profile resulting from $\epsilon_{vol} = 1\%$ is realistic, the horizontal stresses for the Stein-Z10 pile (fully saturated sand) and the SIMOX-8B-H pile (in saturated conditions for 80% of the penetration depth) are compared against those predicted by Equation 4.2. As shown in Figure 4.4, the originally developed for pile Stein-Z10, analytical expression 4.2, results in an increased stress profile along the full length of the pile that is replicated with good agreement by a uniform $\epsilon_{vol} = 1\%$. However, for the longer pile SIMOX-8B-H, Equation 4.2, originally calibrated for shorter piles indicates a reduced post-installation stress state compared to that resulting from $\epsilon_{vol} = 1\%$. This reduction stems from the exponential term in Equation 4.2, which accounts for friction fatigue by applying a decay that scales with the pile penetration depth (PPD). Consequently the larger PPD of SIMOX-8B-H, amplifies the exponential decay, leading to increased friction fatigue and limited stress increase in the upper half of the pile. This behaviour cannot be replicated by even lower than $\epsilon_{vol} = 1\%$ values, as illustrated in 4.4.

However, the analytically predicted stress state is fully replicated by the $K_{0,mod}$ model through Equation 4.4 as illustrated in Figure 4.6. The horizontal stresses at a scaled radial distance of 0.33D, as described in Section 1.5.1, around the pile are increased in both cases, thereby increasing the stiffness, as seen in Figure 4.5, and resulting in improved agreement with the field test, in terms of lateral response, as illustrated in Figure 4.3. It is also observed that horizontal stresses increase with depth, effectively mimicking the installation effect.

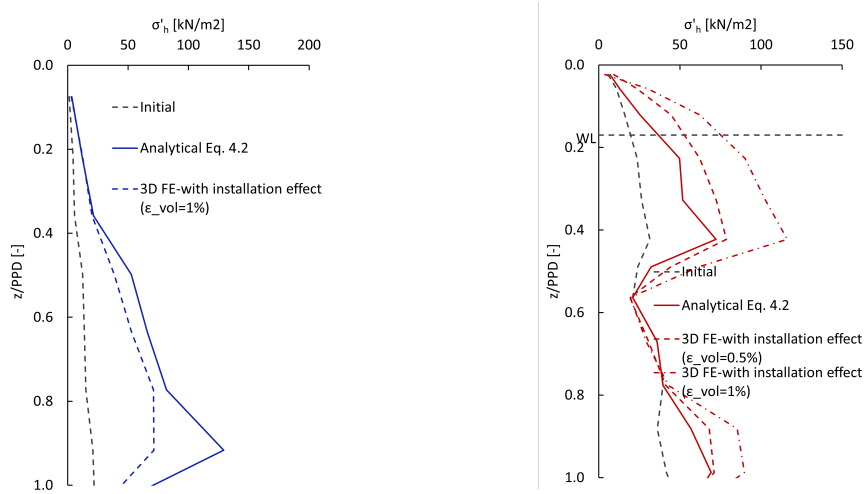

Figure 4.4: Comparison of the analytically predicted and the volumetric strain resulting post-installation stress state at a radial distance of 0.33D from the pile's wall for Stein-Z10 (left) and SIMOX-8B-H (right)

It is important to note that for pile SIMOX-8B-H an evaluation of the horizontal stress agreement should be made only below the waterline level, located at $z/PPD = 0.2$ below the mudline, due to the different stress increase mechanisms described in Chapter 1 and the irrelevance of unsaturated conditions for offshore wind projects. According to [25] installation effects are more pronounced for unsaturated conditions and different values of amplification factor are proposed to account for the intensity of this effect. The values of β for unsaturated conditions were not investigated in this study due to the irrelevance for offshore conditions. For this reason, pile DL1 was only calibrated against the global response.

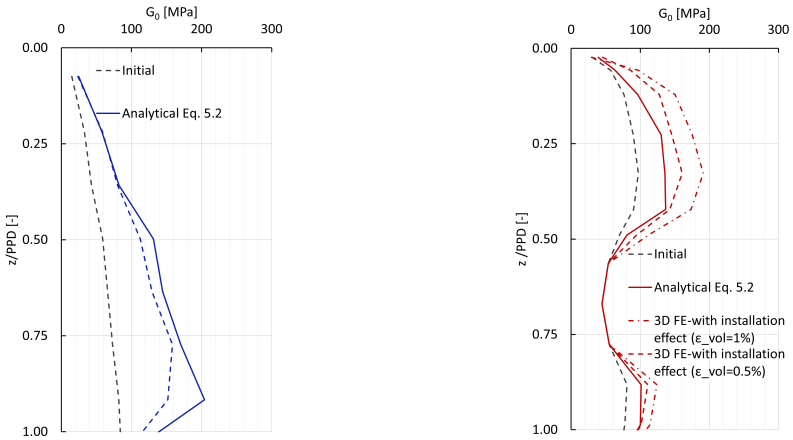

Figure 4.5: Comparison of the post-installation G_0 at a radial distance of 0.33D from the pile's wall as predicted by Equation 4.2 and that resulting from ϵ_{vol} for piles Stein-Z10 (left) and SIMOX-8B-H (right)

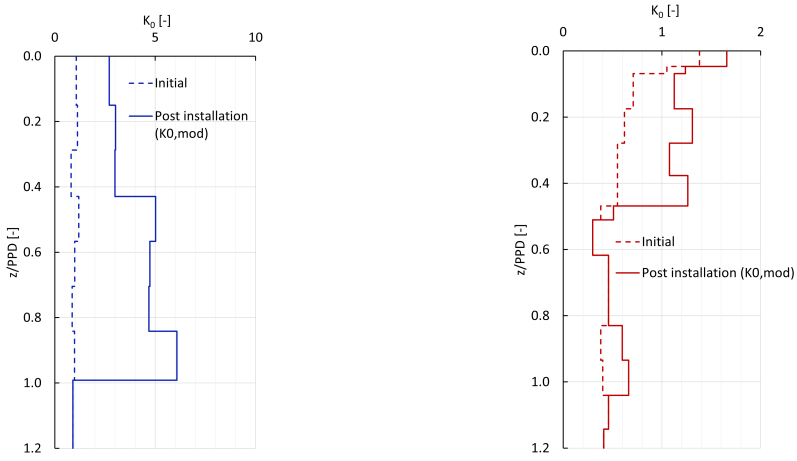

Figure 4.6: Comparison of K_0 profiles pre- and post-installation for Stein-Z10 (left), SIMOX-8B-H (right)

4.2.1 Sensitivity study

In this section a sensitivity study on the effect of volumetric strain for the impact driven pile PISA-DL1 is presented. The results of this are shown in Figure 4.7. The load-displacement curve indicates that an $\epsilon_{vol} = 1\%$ yields the best overall agreement with the field data when the comparison is made for a lateral displacement equal to 2%D at the mudline, which broadly represents the displacement range for FLS and SLS conditions. The figure also shows the diminishing effect of volumetric strains with increasing magnitude but also with increasing strains.

This trend is more evident on the right plot of Figure 4.7, which shows the lateral secant stiffness (K_{sec}) at the mudline for varying volumetric strain values ranging from 0.5 to 3%. The marginal benefit of increasing volumetric strains decreases and the effect is not only diminishing with larger volumetric strain values but also with increasing displacement level. In other words the impact of volumetric strain is greater for small strains and decreases with increasing level of displacements.

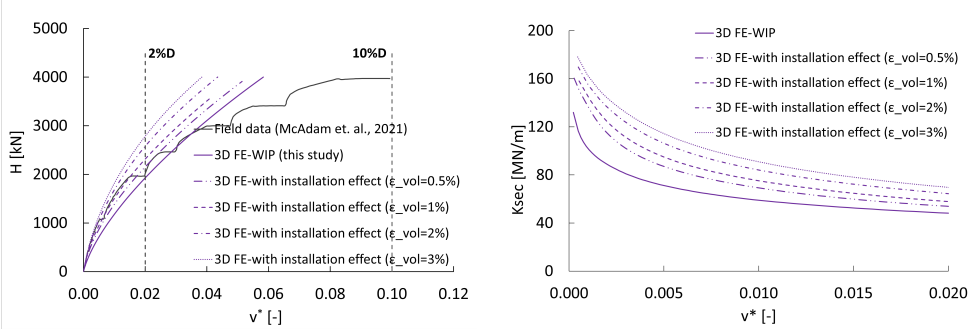

Figure 4.7: Lateral response of PISA-DL1 for varying levels of volumetric strain (left) and lateral secant stiffness for different levels of volumetric strain (right).

4.3 Case study

A case study is performed in this section, to assess the applicability of the proposed methodology in realistic, full-scale conditions, using data from an offshore wind farm in the Dutch North Sea. The site consists of similar soil conditions as those examined throughout this thesis. The relevant geotechnical properties of the soil layers required for applying this method; are summarized in Table C.3, while the basic geometrical properties of the monopile are listed in the following table:

Pile	Project	Installation	D [m]	PPD [m]	t [m]	e [m]
CS1	Case study	Impact	8.0	27.75	0.065	40.0

Table 4.2: Overview of the geometric properties and installation method for monopile CS1

Figure 4.9 indicates that the post-installation stress profiles resulting from Equation 4.2 and that resulting from $\epsilon_{vol} = 1\%$ are not in agreement. However in this case no measured data for the post installation stress state exist that could verify the true post installation stress state. Based on Equation 4.2 the stress increase is localized near the pile toe. Specifically, in the upper quarter of the pile, friction fatigue controls the post-installation stress state resulting in almost no stress increase, while a significant increase is observed close to the pile toe. This stress profile cannot be replicated by the uniform planar volumetric strain approach. In contrast, the $K_{0,\text{mod}}$ model captures the post installation stress state predicted by Equation 4.2 as illustrated in Figure 4.9 and leads to a conservative, yet improved, prediction of the lateral response, as illustrated in Figure 4.8.

Overall, for the full scale pile the $\epsilon_{vol} = 1\%$ increases the stresses across the entire embedment length of the pile and therefore increases the lateral stiffness across the full strain spectrum up to 2%D. On the contrary the $K_{0,\text{mod}}$ approach replicates the stress state changes implied by Equation 4.2 resulting in localized stress increase at the pile of the toe and a more conservative increase of the lateral stiffness for larger strains compared to the volumetric strain method. That can be explained by the by the fact that the ϵ_{vol} increases the stresses also at the upper part of the pile which is mobilized for small strains therefore stiffness increase even from the small strain region. However, the $K_{0,\text{mod}}$ effect is for larger strains since only the properties of the lower soil that is later, for larger strains mobilized, are changed.

In summary, regarding the installation parameters ϵ_{vol} and $K_{0,mod}$ for impact driven monopiles in saturated conditions, it is concluded than an $\epsilon_{vol} = 1\%$ can be adopted as a practical design value for future offshore wind projects in similar soil conditions with those studied herein. This value is calibrated against the lateral response of medium and large scale field tests in predominantly dense sandy soils. This approach can be considered as a progressive approach to capture installation effects, resulting in increased horizontal stresses across the entire penetration depth, opposing to analytical expression and some pressure measurements. The $K_{0,mod}$ approach is calibrated against the analytical expression 4.2, capturing a more localized to the lower part of the pile stress increase as implied by pressure measurements and can

be used as a conservative approach to capture installation effects.

For large (SIMOX) and full-scale (case study) monopiles, the uniform volumetric strain approach generally overestimates the post-installation stress state predicted by the analytical expression. However, since Equation 4.2 has not yet been validated against full-scale pressure measurements, its reliability remains uncertain. Therefore, using $\epsilon_{vol} = 1\%$ is recommended for such applications.

Alternatively, the $K_{0,mod}$ model, which replicates the analytically derived post installation stress state can safely be used as a conservative, yet improved compared to the WIP, method to estimate the lateral response.

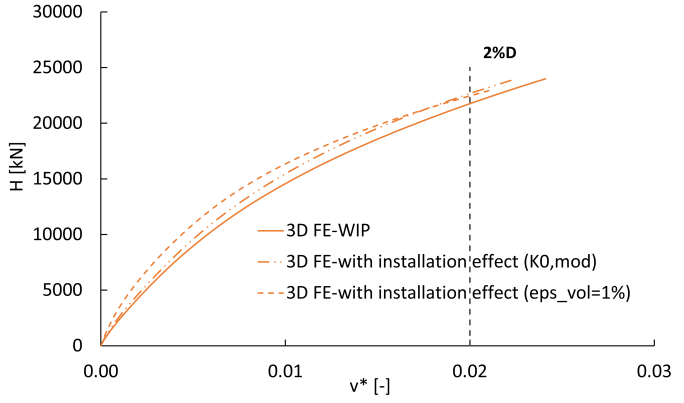

Figure 4.8: Lateral response of pile CS1 with installation effect

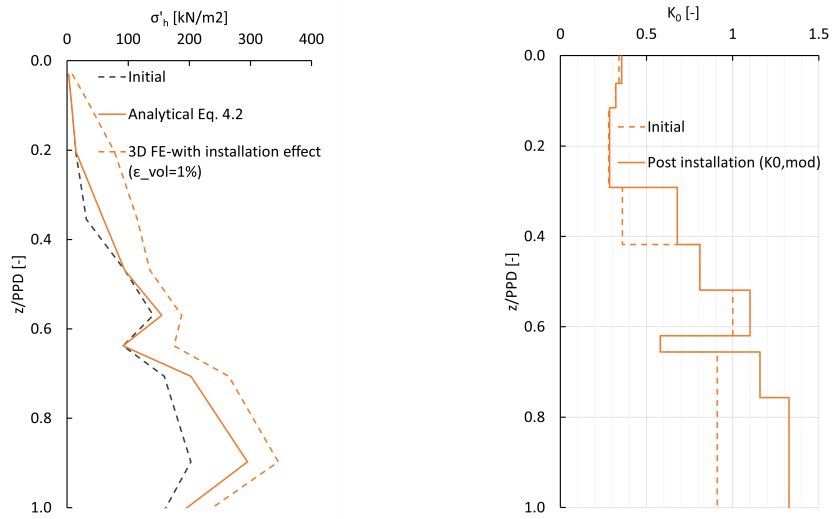

Figure 4.9: Post-installation stress profile at a radial distance of 0.33D from the pile's wall as predicted by Equation 4.2 (solid curve) and that resulting from $\epsilon_{vol} = 1\%$ (dashed curve) for pile CS1 (left). Comparison of K_0 profiles pre- and post-installation for pile CS1 (right)

Chapter 5

Conclusions and recommendations

5.1 Conclusions

In this study the installation effects on the lateral behaviour of impact and vibratory driven monopiles were investigated. The literature review showed that installation effects are present in dense sandy soils and that they can be neglected for piles driven in clay soils. Therefore the lateral response of piles in predominantly dense sandy soils were investigated using FE modelling.

A methodology was first developed to interpret the initial (undisturbed) soil properties, to model the WIP response representing the current industry practice where installation effects are generally ignored. These models served as the reference for the subsequent incorporation of installation effects.

The WIP models underestimate the initial stiffness of impact driven monopiles, while they were able to adequately capture - or in some cases even overpredict - the response of vibratory driven monopiles. It was therefore concluded that vibratory driven monopiles can generally be modelled using the simple WIP models, however installation effects have to be accounted for in the modelling approach of impact driven piles, to accurately predict their lateral response.

The literature review indicated that the increase in effective horizontal stresses

around the pile had the most significant impact on the lateral behaviour. Hence, it was decided to incorporate the effect of installation by modifying the soil properties through the change of horizontal stresses as an efficient way to capture installation effects.

Two different approaches were presented, both leading to improved agreement with the field tests; namely the application of a uniform planar volumetric strain in the soil plug (ϵ_{vol}) or alternatively the modification of the coefficient of lateral earth pressure at rest (K_0). Calibration showed that a uniform $\epsilon_{vol} = 1\%$ leads to excellent agreement with the field response across several medium- and large-scale tests, and could potentially serve as a practical design value for offshore wind projects in the North Sea with similar soil conditions. The resulting stress state from ϵ_{vol} was compared against analytically derived post-installation stress profiles. This comparison indicated that ϵ_{vol} produces higher stresses than those predicted by the analytical expression, leading to different stress distributions for large to full scale applications.

The $K_{0,mod}$ approach was calibrated against the analytically derived post-installation stress state, resulting in stress increase mainly at the lower half of the pile. This produced a stiffer response than the WIP model but generally less stiff than that obtained with the ϵ_{vol} approach. It was found that when appropriately calibrated, both methods could stiffen the response and lead to improved prediction of the lateral response. The absence of calibration of the analytical stress expression against full-scale pressure measurements remains a limitation in this study which introduces uncertainty in similar applications.

The proposed approaches can be used to account for the installation effects on the lateral behaviour of monopile for offshore wind projects, within a generalized framework integrating both the calibration of initial constitutive model parameters and the incorporation of installation effects within a FE-based design workflow, thus leading to improved quality in the prediction of lateral behaviour of monopiles. The improved prediction of foundation stiffness, will lead to a stiffer overall response of the wind turbine and is expected to narrow the observed frequency gap by contributing to a more accurate prediction of the first natural frequency.

5.2 Practical recommendations

A workflow to incorporate installation effects into a FE model is presented in this section. For vibratory-driven monopiles, the WIP model alone is sufficient, as installation effects have been shown to be negligible. In contrast, for impact-driven

monopiles, two alternative strategies are proposed to account for installation effects; namely applying a uniform volumetric strain ϵ_{vol}, or modifying the coefficient of lateral earth pressure ($K_{0,\text{mod}}$). A volumetric strain of $\epsilon_{vol} = 1\%$ has been calibrated against the global response for medium- and large-scale tests. This value can be used as a practical starting point for future offshore wind projects in similar sandy soils. However, its reliability at full scale remains uncertain: while it generally improves model accuracy, it may overestimate the stress state. On the other hand, the $K_{0,\text{mod}}$ approach, derived from an analytical expression, yields a conservative yet improved lateral response, for small strain levels, but has not yet been calibrated against full-scale pressure measurements and is expected to lead to non-conservative results for larger displacement levels, as discussed in 4.1.2. However, both methods, $\epsilon_{vol} = 1\%$ and $K_{0,\text{mod}}$, offer practical ways to incorporate installation effects, with the latter providing a more conservative alternative to the conventional WIP model.

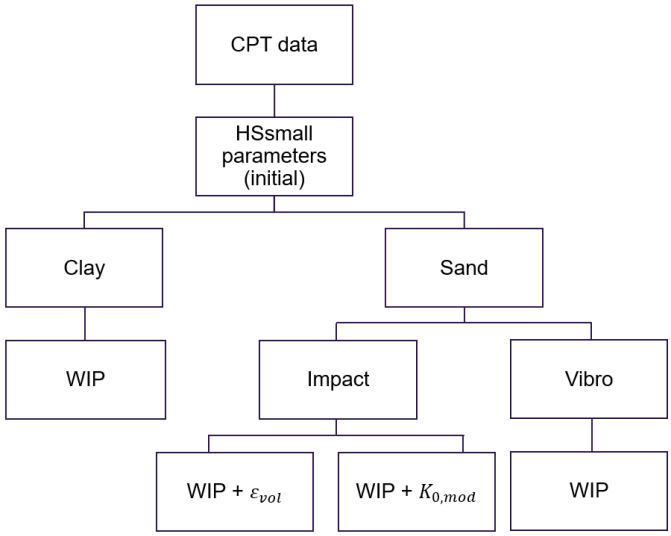

Figure 5.1: Proposed workflow to incorporate installation effects into the modelling approach

5.2.1 Reference envelope for post-installation horizontal stress change

This section summarizes measured post installation stress states from impact-driven pile experiments, providing a reference envelope for evaluating the installation parameters (ϵ_{vol} and $K_{0,mod}$). The tests cover a range of scales from small (SIMOX [20], Stein [48]) to larger (Spill et al. [47]), all conducted in dense saturated dense sand. The results are summarized in Figure 5.2, in the form of post to pre installation horizontal stresses, showing the stress changes due to installation.

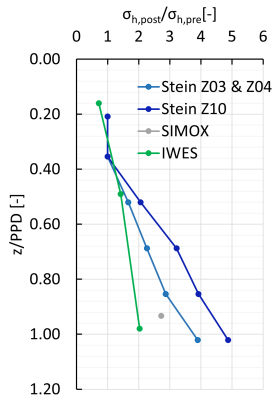

Figure 5.2: Envelope of post-installation horizontal effective stress factors with normalized depth. Data from Stein [48], SIMOX [20], and Spill et al. [47] field tests.

The measurements indicate that the net stress increase, is present below approximately 40% of the pile penetration depth (PPD), increasing with depth. Maximum stress factorsrange from from approximately 2 to 4, for Spill et al. [47] and Stein [48] respectively. The larger stress increase measured in the tests of Stein [48] and da Silva et al. [20] can be attributed to the smaller diameter of the piles used compared to Spill et al. [47], in line with the findings of [25], possibly due to soil plugging. At the upper 40% of the piles the post installation stress state varies from a negligible change for the piles of Stein [48] to a net decrease in the large scale IWES test [47]. The greater PPD in the latter may explain this reduction, implying more pronounced friction fatigue effects. It is also important to mention that the measurements were performed at a different scaled distance from the pile wall (r/D), introducing additional uncertainty.

	Stein-Z03&Z04 [48]	Stein-Z10 [48]	Spill et al. [47]	SIMOX [20]
r/D [-]	0.33	0.33	0.20	0.50
Dr [%]	74	74	68	80
D [m]	0.6	0.6	1.52	0.3
PPD [m]	2.4	2.4	6.15	1.5

Table 5.1: Overview of the geometric properties and installation method for the tests considered in the reference envelope. Note that SIMOX refers to the small-scale part of the SIMOX project.

Nevertheless, these values may be used as a reference for future applications of installation effects, in order to verify the validity of imposed post installation stress profiles, but also highlight the importance of scale effects and the need for full scale tests to verify these findings. An overview of the geometrical characteristics and D_r for the referenced studies is summarized in Table 5.1.

5.3 Recommendations for future studies

Based on the findings and limitations identified in this study, the following recommendations are proposed to further validate, refine and expand the applicability of the proposed methodology for modelling installation effects on monopile foundations:

- Validate the volumetric strain proposed values against the global response of full-scale monopiles in offshore field tests.
- Validate the analytical expression for the post-installation stress profile against pressure measurements from large scale onshore field tests, to verify the applicability of this approach in larger monopiles.
- Develop a continuous closed-form correlation between the stress amplification factor β and the relative density D_r, to improve the reliability of the analytical expression in predicting the post-installation stress state.
- Based on the improved with installation effect FE models, calibrate the stiffness parameters of 1D springs stiffness values to enable simplified 1D modelling that accounts for installation effects.
- Investigate the effect of the improved-stiffer foundation modelling on the natural frequency of various monopile-supported offshore wind turbines.

Bibliography

[1] M. Achmus, M. Terceros, and K. Thieken. Assessment of p-y approaches for piles in normally and over-consolidated soft clay. In *Proceedings of the 27th International Offshore and Polar Engineering Conference (ISOPE)*, pages 570–578, 2017.

[2] Martin Achmus, Klaus Thieken, Jann-Eike Saathoff, Mauricio Terceros, and Johannes Albiker. Un- and reloading stiffness of monopile foundations in sand. *Applied Ocean Research*, 84:62–73, 2019. ISSN 0141-1187. doi: https://doi.org/10.1016/j.apor.2019.01.001. URL https://www.sciencedirect.com/science/article/pii/S014111871830573X.

[3] Martin Achmus, Kirill Schmoor, Volker Herwig, and Ben Matlock. Lateral bearing behaviour of vibro-driven and impact-driven large diameter foundation piles in dense sand. *geotechnik*, 43, 06 2020. doi: 10.1002/gete.202000006.

[4] T. Alm and L. Hamre. Soil model for pile driveability predictions based on cpt interpretations. In *Proceedings of the 15th International Conference on Soil Mechanics and Geotechnical Engineering*, pages 104–107, Istanbul, Turkey, 2001. ISSMGE. URL https://www.issmge.org/uploads/publications/1/30/2001_02_0104.pdf.

[5] I. Alpan. The geotechnical properties of soils. *Earth-Science Reviews*, 6(1):5–49, 1970. ISSN 0012-8252. doi: https://doi.org/10.1016/0012-8252(70)90001-2. URL https://www.sciencedirect.com/science/article/pii/0012825270900012.

[6] Yazeed Alsharedah, Tim Newson, M.Hesahm El Naggar, and Jonathan Black. Lateral ultimate capacity of monopile foundations for offshore wind turbines:

Effects of monopile geometry and soil stiffness properties. *Applied Sciences*, 13, 11 2023. doi: 10.3390/app132212269.

[7] G. Baldi, R. Belotti, N. Ghionna, M. Jamiolkowski, and E. Pasqualini. Interpretation of CPT and CPTU; 2nd part: drained penetration of sands. In *Proceedings of the Fourth International Geotechnical Seminar*, pages 143–156, Singapore, 1986. Paper presented at the Fourth International Geotechnical Seminar.

[8] Graham Barnes. *Soil Mechanics*. Macmillan Education UK, London, 2010. doi: 10.1007/978-0-230-36677-0.

[9] *PLAXIS 3D 2024.2 Reference Manual*. Bentley Systems, 2024. URL `https://communities.bentley.com/products/geotech-analysis/w/plaxis-soilvision-wiki`. Last updated: May 07, 2024.

[10] B. Bienen, J. Mazutti, Fraser Bransby, Pourya Kazemi Esfeh, and M.F. Randolph. Investigating installation and post-installation performance of vibro-driven monopiles in sand: Centrifuge modelling and numerical analysis. pages 1830–1837, 09 2023. doi: 10.3723/CFFK2389.

[11] Britta Bienen, Shengsheng Fan, Maximilian Schröder, and Mark F. Randolph. Effect of the installation process on monopile lateral response. *Proceedings of the Institution of Civil Engineers - Geotechnical Engineering*, 174(5):530–548, 2021. doi: 10.1680/jgeen.20.00219. URL `https://doi.org/10.1680/jgeen.20.00219`.

[12] Sanne Djai Blok. Lateral bearing capacity of gbm vibro-drill installed monopiles: A worst-case scenario analysis. Master's thesis, Delft University of Technology, Delft, The Netherlands, July 2019. URL `https://repository.tudelft.nl/islandora/object/uuid:b7e13f26-6cd3-48d2-93cc-470bb0a40c83`. MSc Thesis, European Wind Energy Master (EWEM) programme.

[13] R. Brinkgreve, Erjona Engin, and Harun Kürşat Engin. Validation of empirical formulas to derive model parameters for sands. 06 2010. ISBN 978-0-415-59239-0. doi: 10.1201/b10551-25.

[14] Harvey Burd, David M. G. Taborda, Lidija Zdravkovic, Christelle Abadie, Byron Byrne, Guy Houlsby, Kenneth Gavin, David Igoe, Richard Jardine, Chris Martin, Ross Mcadam, Antonio Pedro, and David Potts. Pisa design model for monopiles for offshore wind turbines: application to a marine sand. *Géotechnique*, 70:1048–1066, 02 2020. doi: 10.1680/jgeot.18.p.277.

[15] J.B. Burland. Ninth laurits bjerrum memorial lecture: Small is beautiful - the stiffness of soils at small strains. *Canadian Geotechnical Journal*, 26(4):499–516, 1989. doi: 10.1139/t89-064.

[16] Sebastian Matias Bascunan Chaparro. Cpt-based method to determine the lateral capacity of monotonically loaded rigid piles in sand. Msc thesis, Delft University of Technology, Delft, The Netherlands, 2019. Supervisors: Dr. K.G. Gavin, Ir. K. Reinders, Dr. F. Pisanò, Ir. K. Kaltekis, Ir. B.F.J. van Dijk.

[17] Sebastian Matias Bascunan Chaparro. Cpt-based method to determine the lateral capacity of monotonically loaded rigid piles in sand. Msc thesis, Delft University of Technology, Delft, The Netherlands, August 2019. Supervisors: Dr. K.G. Gavin, Ir. K. Reinders, Dr. F. Pisanò, Ir. K. Kaltekis, Ir. B.F.J. van Dijk.

[18] Giuseppe Costanzo, Guy Brindley, and Pierre Tardieu. Wind energy in europe: 2024 statistics and the outlook for 2025–2030, February 2025. URL `https://windeurope.org/intelligence-platform/product/wind-energy-in-europe-2024-statistics-and-the-outlook-for-2025-2030/`. Accessed: 2025-06-21.

[19] Anderson Da Silva, Mark Post, Ahmed Elkadi, Evangelos Kementzetzidis, and Federico Pisanò. Effect of installation parameters and initial soil density on the lateral response of vibratory-driven monopiles: A laboratory study. 09 2023. doi: 10.3723/LFBS1210.

[20] Anderson Peccin da Silva, Martijn Post, Ankit Sharma, Michail Konstantinou, and Ahmed S.K. Elkadi. A numerical modelling exercise to simulate the lateral behaviour of impact and vibro-driven piles in dense sand. In Christelle Abadie, Zheng Li, Matthieu Blanc, and Luc Thorel, editors, *Proceedings of the 5th International Symposium on Frontiers in Offshore Geotechnics (ISFOG 2025)*, Nantes, France, June 9–13 2025. ISSMGE. URL `https://www.issmge.org/publications/online-library`. Paper No. 584.

[21] M. Damgaard, M. Bayat, Lars Andersen, and Lars Ibsen. Assessment of the dynamic behaviour of saturated soil subjected to cyclic loading from offshore monopile wind turbine foundations. *Computers and Geotechnics*, 61:116–126, 09 2014. doi: 10.1016/j.compgeo.2014.05.008.

[22] GL Dnv. Dnvgl-st-0126: Support structures for wind turbines. *Oslo, Norway: DNV GL*, 632, 2016.

[23] Shengsheng Fan, Britta Bienen, and Mark Randolph. Effects of monopile installation on subsequent lateral response in sand. i: Pile installation. *Journal of Geotechnical and Geoenvironmental Engineering*, 147:04021021, 03 2021. doi: 10.1061/(ASCE)GT.1943-5606.0002467.

[24] Sakineh Fazlighiyasabadi, Majid Goodarzi, Majid Fetrati, Stefan Kreiter, Vahid Galavi, Lars Bo Ibsen, Junyu Zhou, Søren Peder Hyldal Sørensen, Cesar Garcia Quirante, Pooyan Ghasemi, and Tobias Mörz. Practical considerations for numerical simulation of large-diameter monopiles for offshore wind turbines in overconsolidated sand: A case study of the vibro project in cuxhaven, germany. *Ocean Engineering*, 313:119365, 2024. ISSN 0029-8018. doi: https://doi.org/10.1016/j.oceaneng.2024.119365. URL `https://www.sciencedirect.com/science/article/pii/S0029801824027033`.

[25] Jan Fischer. *Ramminduzierte Spannungsfeldänderungen im Nahbereich von Rohrprofilen großen Durchmessers*. PhD thesis, 02 2021.

[26] Jörg Gattermann, Volker Herwig, and Christian Moormann. Vibro project – vergleich des lateralen tragverhaltens von vibrierten und geschlagenen stahlrohrpfählen in sandigen böden. In *Pfahl-Symposium 2015, Mitteilungen des Instituts für Grundbau und Bodenmechanik, Heft 99*, Braunschweig, Germany, 2015.

[27] Kenneth Gavin, S.D. Blok, and G.R. Eiksund. The impact of installation method on monotonic loading of monopiles in sand. In Zack Westgate, editor, *Proceedings Fourth International Symposium on Frontiers in Offshore Geotechnics*, pages 849–857, 2020. URL `https://www.isfog2020.org/`.

[28] Susan Gourvenec and Mark Randolph. *Offshore Geotechnical Engineering*. 01 2011. ISBN ISBN 13: 9780415477444 ISBN 10: 0415477441. doi: 10.1201/9781315272474.

[29] Bastian Hoffmann, Johannes Labenski, and Christian Moormann. Effects of vibratory driving of monopiles on soil conditions and their cyclic lateral load bearing behavior. 09 2020.

[30] Qian Hu, Fei Han, Monica Prezzi, Rodrigo Salgado, and Minghua Zhao. Finite-element analysis of the lateral load response of monopiles in layered sand. *Journal of Geotechnical and Geoenvironmental Engineering*, 148, 04 2022. doi: 10.1061/(ASCE)GT.1943-5606.0002745.

[31] Sachin Jindal, Ulvi Rahmanli, Muhammad Aleem, Liang Cui, and Subhamoy Bhattacharya. Geotechnical challenges in monopile foundations and performance assessment of current design methodologies. *Ocean Engineering*, 310: 118469, 2024. ISSN 0029-8018. doi: https://doi.org/10.1016/j.oceaneng.2024.118469. URL https://www.sciencedirect.com/science/article/pii/S0029801824018079.

[32] Dan Kallehave, Byron Byrne, Christian Thilsted, and Kristian Mikkelsen. Optimization of monopiles for offshore wind turbines. *Philosophical transactions. Series A, Mathematical, physical, and engineering sciences*, 373, 02 2015. doi: 10.1098/rsta.2014.0100.

[33] Max Kluger, Majid Goodarzi, Stefan Kreiter, Pooyan Ghasemi, Taisiya Pein, and Tobias Mörz. Influence of sample reconstitution on advanced model calibration. *International Journal of Geomechanics*, 22, 05 2022. doi: 10.1061/(ASCE)GM.1943-5622.0002498.

[34] Haoyuan Liu, Evangelos Kementzetzidis, José Antonio Abell, and Federico Pisanò. From cyclic sand ratcheting to tilt accumulation of offshore monopiles: 3d fe modelling using sanisand-ms. *Géotechnique*, 72(9):753–768, 2022. doi: 10.1680/jgeot.20.P.029. URL https://doi.org/10.1680/jgeot.20.P.029.

[35] J. Machaček, J. Liaudat, S. Siegel, and H. Zachert. Blind prediction contest: Piles under monotonic and cyclic lateral loading. In *Proceedings of the 5th International Symposium on Frontiers in Offshore Geotechnics (ISFOG)*, Nantes, France, 2025. International Society for Soil Mechanics and Geotechnical Engineering (ISSMGE). ISBN 978-2-85782-758-0. URL https://www.issmge.org/publications/online-library.

[36] Ross Mcadam, Byron Byrne, Guy Houlsby, William Beuckelaers, Harvey Burd, Kenneth Gavin, David Igoe, Richard Jardine, Chris Martin, Alastair Wood, David Potts, Jesper Gretlund, David M. G. Taborda, and Lidija Zdravkovic. Monotonic laterally loaded pile testing in a dense marine sand at dunkirk. *Géotechnique*, 70:986–998, 11 2019. doi: 10.1680/jgeot.18.pisa.004.

[37] E. Minga and H. J. Burd. Validation of the plaxis modeto 1d model for dense sand. Technical report, Oxford University, Oxford, UK, 2019.

[38] Majid Movahedi Rad. Reliability based analysis and optimum design of laterally loaded piles. *Periodica Polytechnica Civil Engineering*, 61, 01 2017. doi: 10.3311/PPci.8756.

[39] A. Nernheim, P. Voges-Espelage, C. H. Wilsch, S. Panagoulias, A. Iliopoulos, S. J. Hermans, and P. Versteijlen. Soil modelling impact on the natural frequency of offshore wind turbines with reference to in-field measurements. In Christelle Abadie, Zheng Li, Matthieu Blanc, and Luc Thorel, editors, *Proceedings of the 5th International Symposium on Frontiers in Offshore Geotechnics (ISFOG 2025)*, pages 403–410, Nantes, France, June 9–13 2025. ISSMGE. URL `https://www.issmge.org/uploads/publications/132/133/ISFOG2025-403.pdf`.

[40] S. Panagoulias, R. B. J. Brinkgreve, and L. Zampich. *PLAXIS MoDeTo Manual 2018*. Plaxis bv – a Bentley Systems company, Delft, The Netherlands, 2018.

[41] Stavros Panagoulias, Axel Nernheim, Diego Lisi, Miquel Lahoz, and R. Brinkgreve. Concept design study of laterally loaded monopiles in sand. 08 2020.

[42] F. Pisanò, I. Del Brocco, H.M. Ho, and S. Brasile. 3d fe simulation of pisa monopile field tests at dunkirk using sanisand-ms. *Geotechnique Letters*, 14(2): 35–45, 2024. ISSN 2045-2543. doi: 10.1680/jgele.23.00073.

[43] Santiago Quinteros, Tom Lunne, Lone Krogh, R Bøgelund-Pedersen, and Jens Brink Clausen. Shallow depth characterisation and stress history assessment of an over-consolidated sand in cuxhaven, germany. 06 2018.

[44] Peter K. J. Robertson. Performance based earthquake design using the cpt. 2009. URL `https://api.semanticscholar.org/CorpusID:132827052`.

[45] J. H. Schmertmann. Use of SPT to measure dynamic soil properties? Yes, but. . . ! In *Dynamic Geotechnical Testing*, volume 654 of *ASTM Special Technical Publication*, pages 341–355. ASTM International, 1978.

[46] H. B. Seed and I. M. Idriss. Soil moduli and damping factors for dynamic response analyses. Technical Report EERC 70-10, University of California, Berkeley, Berkeley, CA, 1970.

[47] S. Spill, C. Lillie, and M. Collmann. Numerical model of a large-scale monopile test in non-cohesive soil. pages 1622–1628, 09 2023. doi: 10.3723/JWKP7538.

[48] Philipp Stein. *Stress state developments during the installation of pipe piles in sand and their influence on the lateral load-bearing behaviour*. PhD thesis, 02 2023.

[49] Philipp Stein. Stress effects due to different installation methods for pipe piles in sand. *Proceedings of the Institution of Civil Engineers - Geotechnical Engineering*, 177(5):533–545, 2024. ISSN 1353-2618. doi: https://doi.org/10.1680/jgeen.23.00105. URL https://www.sciencedirect.com/science/article/pii/S1353261824000310.

[50] David M. G. Taborda, Lidija Zdravkovic, David Potts, Harvey Burd, Byron Byrne, Kenneth Gavin, Guy Houlsby, Richard Jardine, Tingfa Liu, Chris Martin, and Ross Mcadam. Finite-element modelling of laterally loaded piles in a dense marine sand at dunkirk. *Géotechnique*, 70:1014–1029, 11 2019. doi: 10.1680/jgeot.18.pisa.006.

[51] Klaus Thieken, Martin Achmus, and Katrin Lemke. A new static p-y approach for piles with arbitrary dimensions in sand. *geotechnik*, 38:267–288, 12 2015. doi: 10.1002/gete.201400036.

[52] Frits Tol and Wout Broere. Modelling the bearing capacity of displacement piles in sand. *Proceedings of The Institution of Civil Engineers-geotechnical Engineering - PROC INST CIVIL ENG-GEOTECH E*, 159:195–206, 01 2006. doi: 10.1680/geng.2006.159.3.195.

[53] Athanasios Tsetas, Apostolos Tsouvalas, Sergio S. Gómez, Federico Pisanò, Evangelos Kementzetzidis, Timo Molenkamp, Ahmed S.K. Elkadi, and Andrei V. Metrikine. Gentle driving of piles (gdp) at a sandy site combining axial and torsional vibrations: Part i - installation tests. *Ocean Engineering*, 270:113453, 2023. ISSN 0029-8018. doi: https://doi.org/10.1016/j.oceaneng.2022.113453. URL https://www.sciencedirect.com/science/article/pii/S0029801822027366.

[54] Apostolos Tsouvalas. Underwater noise emission due to offshore pile installation: A review. *Energies*, 13(12), 2020. ISSN 1996-1073. doi: 10.3390/en13123037. URL https://www.mdpi.com/1996-1073/13/12/3037.

[55] W. Versteijlen, J. De oliveira Barbosa, K. van Dalen, and A. Metrikine. Method for extracting an equivalent winkler model of the 3d dynamic soil-structure interaction of large diameter offshore monopile foundations. In *Proceedings of 43th International Summer School-Conference Advanced Problems in Mechanics (APM)*, 2015. URL https://www.ipme.ru/ipme/conf/APM2015/2015-PDF/2015-436.pdf.

[56] W G Versteijlen, K N van Dalen, A V Metrikine, and L Hamre. Assessing the small-strain soil stiffness for offshore wind turbines based on in situ seismic measurements. *Journal of Physics: Conference Series*, 524(1):012088, jun 2014. doi: 10.1088/1742-6596/524/1/012088. URL https://dx.doi.org/10.1088/1742-6596/524/1/012088.

[57] Lidija Zdravkovic, David M. G. Taborda, David Potts, David Abadias, Harvey Burd, Byron Byrne, Kenneth Gavin, Guy Houlsby, Richard Jardine, Chris Martin, Ross Mcadam, and Emil Ushev. Finite-element modelling of laterally loaded piles in a stiff glacial clay till at cowden. *Géotechnique*, 70:999–1013, 11 2019. doi: 10.1680/jgeot.18.pisa.005.

[58] Youhu Zhang and Knut H. Andersen. Soil reaction curves for monopiles in clay. *Marine Structures*, 65:94–113, 2019. ISSN 0951-8339. doi: https://doi.org/10.1016/j.marstruc.2018.12.009. URL https://www.sciencedirect.com/science/article/pii/S0951833918300698.

Appendix A

Soil Properties

A.1 Soil Profiles

This section presents the soil profiles for the investigated field tests.

z_{Top} [m]	z_{Bottom} [m]	Soil Type	Dr [%]
0.00	0.43	sand	89
0.43	0.68	sand	116
0.68	0.99	sand	120
0.99	2.10	sand	120
2.10	2.64	sand	108
2.64	3.52	sand	89
3.52	3.72	sand	111
3.72	4.28	sand	115
4.28	4.58	sand	103
4.58	6.45	sand	96
6.45	8.44	sand	87
8.44	8.99	sand	89
8.99	10.10	sand	99
10.10	12.00	sand	99

Table A.1: Soil stratigraphy, type and relative densities for piles DM4, DM7, DL1 (PISA field test) [57]

z_{Top} [m]	z_{Bottom} [m]	Soil Type	Dr [%]
0.00	1.13	sand	71
1.13	2.72	sand	83
2.72	3.70	sand	80
3.70	5.06	sand	51
5.06	5.59	sand	79
5.59	7.46	sand	93
7.46	9.35	sand	87
9.35	11.25	sand	75
11.25	13.17	sand	66
13.17	14.00	sand	80
14.00	15.68	sand	72
15.68	17.55	sand	52
17.55	20.00	sand	52

Table A.2: Soil stratigraphy, type and relative densities for pile P2h (Cuxhaven field test) [3]

z_{Top} [m]	z_{Bottom} [m]	Soil Type	Dr [%]
0.00	0.32	sand	63
0.32	1.48	sand	94
1.48	3.11	sand	82
3.11	4.21	sand	59
4.21	5.13	clay	-
5.13	5.49	sand	77
5.49	7.26	sand	84
7.26	9.12	sand	79
9.12	11.07	sand	75
11.07	12.76	sand	66
12.76	13.7	sand	80
13.7	14.17	sand	89
14.17	14.76	sand	77
14.76	15.57	sand	87
15.57	16.1	sand	46
16.1	17.99	sand	50
17.99	20	sand	50

Table A.3: Soil stratigraphy, type and relative densities for pile P1v (Cuxhaven field test) [3]

z_{Top} [m]	z_{Bottom} [m]	Soil Type	Dr [%]
0.00	0.36	sand	72
0.36	0.69	sand	95
0.69	1.03	sand	105
1.03	1.36	sand	104
1.36	2.69	sand	110
1.69	2.02	sand	114
2.02	2.38	sand	111
2.38	2.75	sand	109
2.75	3.00	sand	109

Table A.4: Soil stratigraphy, type and relative densities for pile Z10 (Stein [48])

A.2 HSsmall material model parameters

Below the constitutive model parameters that were used for the validation and analysis of the field tests are presented.

A.2.1 PISA model

The soil properties were calibrated against the original in-situ and laboratory data for the Dunkirk site as reported by [57], [50] and [37].According to the original PISA study, the Dunkirk sand is normally consolidated (NC), and the soil's stratigraphy consists of a hydraulically filled upper layer and a natural deposit of dense marine sand below. According to the interpretation scheme presented in Chapter 3 the constitutive model properties were derived based on in-situ testing. However pile specific CPTs were not available, instead the same CPT trend was used for every pile investigated. That is believed to introduce some uncertainty into the FE model and the interpretation of the constitutive model parameters, since any soil variability among the different locations where the pile were installed cannot be captured. Regarding the modelling it is important to mention that an artificial cohesion was assumed in the first six layers - up to a depth of 6.45 m - in accordance with the original papers by [57] and the modelling approach of [37] to account for uncertainties and the increased strength of the hydraulically filled layer that was found on the Dunkirk site. The water table is reportedly located at 5.4 m below the mudline level, however in this study, it is considered to be at 6.45 m instead; that is not expected to significantly affect the lateral behaviour of the monopiles.

The constitutive model properties by Minga and Burd [37] that were used for validation of the model, are summarized in the following Table A.5. These, together with the HSsmall properties that were derived using the interpretations following from the correlations of Brinkgreve et al. [13] were used to assess the adequacy of the interpretation scheme proposed in this study.

Table A.5: HSsmall material model properties according to C1 interpretation by Minga and Burd [37] used for validation purposes

z_{Top} [m]	z_{Bot} [m]	Drainage [-]	γ' [kN/m^3]	OCR [-]	K_0 [-]	φ' [deg]	c' [kN/m^2]	ψ [deg]	E_{50}^{ref} [kN/m^2]	E_{oed}^{ref} [kN/m^2]	E_{ur}^{ref} [kN/m^2]	G_0^{ref} [kN/m^2]	$\gamma_{0.7}$ [-]	ν_{ur} [-]	ϕ'_{inter} [deg]
0	3.0	0	17.1	1	0.4	44	5.0	15	60000	60000	460633	196852	1.00E-04	0.17	29
3.0	5.4	0	17.1	1	0.4	40	10.0	10	60000	60000	397040	169675	1.25E-04	0.17	29
5.4	10.0	0	19.9	1	0.4	40	0.1	10	60000	60000	388155	165878	1.25E-04	0.17	29
10.0	20.0	0	19.9	1	0.4	40	0.1	10	60000	60000	367376	156998	1.25E-04	0.17	29

Note: In the Drainage column, 0 = drained. All stiffness values correspond to $p_{ref} = 100$ kPa and stress dependency factor $m = 0.5$

Table A.6: HSsmall material model parameters for PISA field test, correlations from Brinkgreve et al. [13]

z_{Top} [m]	z_{Bot} [m]	Drainage [-]	γ' [kN/m^3]	OCR [-]	K_0 [-]	φ' [deg]	c' [kN/m^2]	ψ [deg]	E_{50}^{ref} [kN/m^2]	E_{oed}^{ref} [kN/m^2]	E_{ur}^{ref} [kN/m^2]	G_0^{ref} [kN/m^2]	$\gamma_{0.7}$ [-]	m [-]	ν_{ur} [-]	ϕ'_{inter} [deg]
0	3.0	0	19.0	1	0.4	40.5	5.0	10.5	60000	60000	180000	128000	1.00E-04	0.39	–	29
3.0	5.4	0	18.0	1	0.4	37.4	10.0	7.37	45000	45000	135000	111000	1.25E-04	0.46	–	29
5.4	10.0	0	20.2	1	0.4	37.4	0.1	7.37	45000	45000	135000	111000	1.25E-04	0.46	–	29
10.0	20.0	0	21.5	1	0.4	37.4	0.1	7.37	45000	45000	135000	111000	1.25E-04	0.46	–	29

Note: In the Drainage column, 0 = drained. All stiffness values are at $p_{ref} = 100$ kPa.

Table A.7: HSsmall material model properties according to the NC interpretation of this study, for piles DM4, DM7 and DL1

z_{Top} [m]	z_{Bot} [m]	Drainage [-]	γ' [kN/m^3]	OCR [-]	K_0 [-]	φ' [deg]	c' [kN/m^2]	ψ [deg]	E_{50}^{ref} [kN/m^2]	E_{oed}^{ref} [kN/m^2]	E_{ur}^{ref} [kN/m^2]	G_0^{ref} [kN/m^2]	$\gamma_{0.7}$ [-]	ν_{ur} [-]	R_{inter} [-]
0	0.43	0	18.16	1	0.33	42	5	12	27100	21600	81200	195000	1.00E-05	0.25	0.67
0.43	0.68	0	20.14	1	0.29	45.5	5	15.5	34100	27300	102300	250900	1.00E-05	0.22	0.67
0.68	0.99	0	20.96	1	0.28	46	5	16	35200	28200	105600	259900	4.00E-05	0.22	0.67
0.99	2.1	0	21.5	1	0.28	46	5	16	89100	71200	267200	259900	6.00E-05	0.22	0.67
2.1	2.64	0	21.04	1	0.30	44.5	5	14.5	87400	69900	262300	234500	8.00E-05	0.23	0.67
2.64	3.52	0	20.38	1	0.33	42	5	12	73700	58900	221100	194700	1.00E-05	0.25	0.67
3.52	3.72	0	21.48	1	0.29	45	10	15	89300	71400	267900	240300	1.00E-05	0.23	0.67
3.72	4.28	0	21.76	1	0.29	45.5	10	15.5	92400	73900	277200	249300	1.00E-05	0.22	0.67
4.28	4.58	0	21.29	1	0.31	44	10	14	83500	66800	250500	223300	1.00E-05	0.23	0.67
4.58	6.45	0	21.18	1	0.32	43	10	13	78900	63100	236600	209700	1.30E-04	0.24	0.67
6.45	8.44	0	10.89	1	0.33	42	0.1	12	72400	57900	217100	191300	1.60E-04	0.25	0.67
8.44	8.99	0	11.1	1	0.33	42	0.1	12	74200	59300	222500	196000	1.60E-04	0.25	0.67
8.99	10.1	0	11.57	1	0.31	43.5	0.1	13.5	80900	64800	242800	215800	1.50E-04	0.24	0.67
10.1	12	0	11.57	1	0.31	43.5	0.1	13.5	80900	64800	242800	215800	1.50E-04	0.24	0.67

Note: All stiffness values are provided at reference pressure $p_{ref} = 100$ kPa and stress dependency factor $m = 0.5$. In the Drainage column, 0 = drained.

It is important to mention at this point that although the site was originally characterized as normally consolidated, other studies [30], [17] as well as the original

CPT data and the uncertainty regarding the properties of the top layer may justify overconsolidated (OC) conditions. An OC interpretation of the soil results in the soil properties given in Table A.8 and yield improved agreement with the original field tests, while removing the need to incorporate installation effects into the model. The load-displacement curves for the OC calibrated DM4 and DL1 piles are illustrated in Figure A.1.

Table A.8: Alternative HSsmall material model properties for piles DM4, DL1 according to the OC interpretation of this study.

z_{bot} [m]	γ' [kN/m^3]	OCR [-]	K_0 [-]	φ' [deg]	c' [kN/m^2]	ψ [deg]	E_{50}^{ref} [kN/m^2]	E_{oed}^{ref} [kN/m^2]	E_{ur}^{ref} [kN/m^2]	G_0^{ref} [kN/m^2]	$\gamma_{0.7}$ [-]	ν_{ur} [-]	R_{inter} [-]
0.43	18.16	8	1.35	40.5	0.1	10.5	20600	16500	61900	147500	5E-5	0.26	0.67
0.68	20.14	8	1.30	43.5	0.1	13.5	25200	20100	75500	183000	6E-5	0.24	0.67
0.99	20.96	8	1.27	45.0	0.1	15.0	72000	57600	216000	196200	7E-5	0.23	0.67
2.10	21.50	5.8	1.00	45.5	0.1	15.5	68400	54700	205300	184600	7E-5	0.22	0.67
2.64	21.04	4.1	0.82	43.5	0.1	13.5	63900	51100	191800	170400	9E-5	0.24	0.67
3.52	20.38	3.4	0.75	41.5	0.1	11.5	56500	45200	169400	148800	1.2E-4	0.25	0.67
3.72	21.48	3.0	0.66	44.0	0.1	14.0	69100	55200	207200	184700	1.1E-4	0.23	0.67
4.28	21.76	2.8	0.62	44.5	0.1	14.5	72300	57800	216900	193900	1.1E-4	0.23	0.67
4.58	21.29	2.6	0.61	43.0	0.1	13.0	66700	53300	200000	177200	1.2E-4	0.24	0.67
6.45	21.18	2.3	0.57	42.5	0.1	12.5	65000	52000	194900	172200	1.4E-4	0.24	0.67
8.44	10.89	2.1	0.55	41.5	0.1	11.5	60900	48700	182800	166000	1.7E-4	0.25	0.67
8.99	11.10	2.0	0.53	40.5	0.1	12.0	63300	50600	189800	167200	1.7E-4	0.25	0.67
10.10	11.57	1.9	0.50	43.0	0.1	13.0	69100	55300	207300	183700	1.6E-4	0.24	0.67
12.00	11.57	1.9	0.50	43.0	0.1	13.0	69100	55300	207300	183700	1.6E-4	0.24	0.67

Note: All stiffness values are referenced at $p_{ref} = 100$ kPa and stress dependency factor $m = 0.5$. All layers are modelled as drained.

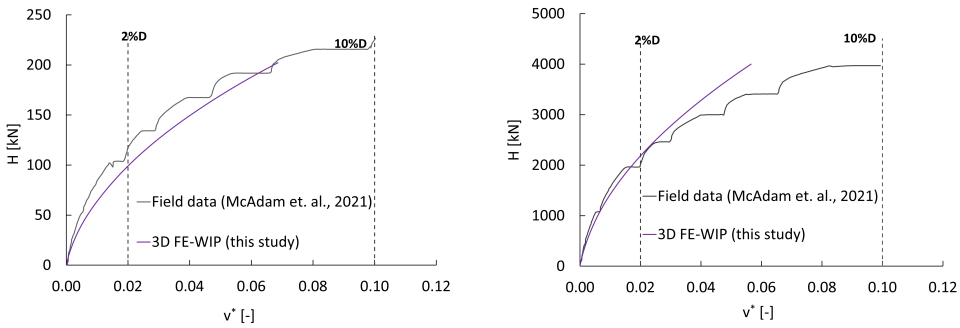

Figure A.1: Alternative lateral response of piles PISA-DM4 (left) and PISA-DL1 (right) according to the OC interpretation.

A.2.2 VIBRO-Cuxhaven model

The original paper of [3] together with supporting studies from [24], [33], [43] were consulted in order to interpret the soil properties in Cuxhaven. Two different pile specific interpretations were performed to account for soil variability and reduce uncertainty, for piles P2h and P1v, based on pile specific CPT, SCPT and sampling data. A conservative pre-overconsolidation pressure of 150 kPa was assumed for the OCR calculation.

The resulting HSsmall model parameters obtained following the approach proposed in this study are presented in Tables A.10 and A.11. These soil profiles were used in the WIP FE models to simulate the response of Cuxhaven piles. The soil properties that were used for the validation of this model according to [24] are also given in Table A.9.

The soil properties of the clay layers were defined as a function of the undrained shear strength (s_u) based on the following formula proposed by [22].

$$G_0 = 600 s_u - 170 s_u \sqrt{OCR - 1} \tag{A.1}$$

Note that for clay layers HSsmall reference properties are equal to absolute stiffness properties; namely there is no stress dependency, owing to the effective angle of internal friction being equal to zero.

Table A.9: HSsmall material model properties for pile P2h of VIBRO-Cuxhaven according to Fazlighiyasabadi et al. [24]

z_{Bot} [m]	γ' [kN/m^3]	OCR [-]	K_0 [-]	φ' [deg]	c' [kN/m^2]	s_u [kN/m^2]	ψ [deg]	E_{50}^{ref} [kN/m^2]	$E_{\text{oed}}^{\text{ref}}$ [kN/m^2]	$E_{\text{ur}}^{\text{ref}}$ [kN/m^2]	G_0^{ref} [kN/m^2]	$\gamma_{0.7}$ [-]	m [-]	ν_{ur} [-]	φ'_{Inter} [deg]
4.4	18.12	3.90	1.44	40	0.1	–	6.1	24960	43680	148200	159000	1.2E-4	0.79	0.25	28.07
5.6	10.44	3.00	0.74	–	0.1	45	–	13484	13484	40453	16181	4.5E-4	1.00	0.25	28.07
7.5	10.71	5.85	1.08	41	0.1	–	8	30400	53200	180500	175200	1.1E-4	0.79	0.25	29.36
10.1	10.58	3.78	0.90	41	0.1	–	7.0	27840	48720	165300	132100	1.1E-4	0.79	0.25	28.30
13.2	10.44	2.89	0.76	40	0.1	–	5.7	29620	43680	148200	255000	1.2E-4	0.79	0.25	27.07
14.6	10.44	2.89	0.70	39	0.1	–	5.7	22400	39200	133000	229000	1.3E-4	0.79	0.25	27.49
16.3	9.83	2.00	0.62	–	0.1	140	–	50568	50568	151704	–	–	–	–	–
18.5	10.73	3.44	0.75	42	0.1	–	8	30720	53760	182400	156200	1.0E-4	0.79	0.26	29.38
21.0	10.73	3.44	0.75	412	0.1	–	8	30720	53760	182400	156200	1.0E-4	0.79	0.26	29.38

Note: Missing values (–) represent parameters not assigned or not applicable. All stiffness values are referenced at $p_{\text{ref}} = 100$ kPa.

Table A.10: HSsmall material model properties per soil layer for pile P1v of Cuxhaven according to the OC interpretation of this study

z_{Top} [m]	z_{Bot} [m]	Drainage [-]	γ' [kN/m^3]	OCR [-]	K_0 [-]	φ' [deg]	c' [kN/m^2]	s_u [kN/m^2]	ψ [deg]	E_{50}^{ref} [kN/m^2]	E_{oed}^{ref} [kN/m^2]	E_{ur}^{ref} [kN/m^2]	G_0^{ref} [kN/m^2]	$\gamma_{0.7}$ [-]	ν_{ur} [-]	R_{inter} [-]
0.00	0.32	0	17.37	8.0	1.37	39.0	0.1	–	9.0	18500	14800	55500	131100	5.0E-05	0.27	0.67
0.32	1.48	0	20.23	4.3	0.89	43.0	0.1	–	11.0	46200	36900	138500	173600	8.0E-05	0.28	0.67
1.48	3.11	0	20.2	4.3	0.89	41.5	0.1	–	11.5	54800	43800	144300	144300	1.0E-04	0.25	0.67
3.11	4.21	0	19.4	3.7	0.79	38.5	0.1	–	9.0	36800	28800	110400	126600	1.2E-04	0.27	0.67
4.21	5.13	0	9.28	2.9	0.74	–	0.1	45	–	34600	27000	39402	166500	1.3E-04	0.26	0.5
5.13	5.49	0	9.12	2.5	0.68	40.5	0.1	–	10.5	59700	49600	167100	149500	1.4E-04	0.26	0.67
5.49	7.26	0	10.64	2.0	0.63	41.5	0.1	–	11.0	57900	47900	175900	150400	1.6E-04	0.26	0.67
7.26	9.12	0	10.55	2.3	0.59	41.0	0.1	–	11.0	58400	46700	173500	154000	1.6E-04	0.26	0.67
9.12	11.07	0	10.24	2.0	0.56	40.5	0.1	–	10.0	52100	41700	164500	135800	2.0E-04	0.27	0.67
11.07	12.76	0	10.24	2.0	0.55	39.5	0.1	–	9.5	52700	41700	164500	138500	2.0E-04	0.27	0.67
12.76	14.76	0	9.79	1.9	0.53	42.0	0.1	–	10.5	59600	47700	171400	156500	1.8E-04	0.25	0.67
14.76	15.76	0	9.73	1.9	0.53	42.0	0.1	–	10.5	59600	47700	171400	156500	1.8E-04	0.25	0.67
15.76	17.39	0	9.74	1.7	0.54	37.5	0.1	–	7.5	23900	23400	87800	122800	2.9E-04	0.28	0.67
17.39	20.00	0	9.74	1.7	0.54	37.5	0.1	–	7.5	23900	23400	87800	122800	2.9E-04	0.28	0.67

Note: Missing values (–) denote parameters not defined for specific layers. Stiffness parameters are referenced at $p_{ref} = 100$ kPa. In the Drainage column, 0 = drained.

Table A.11: HSsmall material model properties per soil layer for pile P1v of Cuxhaven according to the OC interpretation of this study

z_{Top} [m]	z_{Bot} [m]	Drainage [-]	γ' [kN/m^3]	OCR [-]	K_0 [-]	φ' [deg]	c' [kN/m^2]	ψ [deg]	E_{50}^{ref} [kN/m^2]	E_{oed}^{ref} [kN/m^2]	E_{ur}^{ref} [kN/m^2]	G_0^{ref} [kN/m^2]	$\gamma_{0.7}$ [-]	ν_{ur} [-]	R_{inter} [-]
0.00	1.13	0	18.79	8.0	1.36	40.0	0.1	10.0	20000	16000	60000	142400	8.0E-5	0.26	0.67
1.13	2.72	0	20.17	5.0	0.98	41.5	0.1	10.0	54600	43700	163700	143800	9.0E-5	0.25	0.67
2.72	3.70	0	20.34	3.4	0.76	41.0	0.1	11.0	55900	44800	167800	147000	1.0E-4	0.26	0.67
3.70	5.06	0	9.13	2.9	0.75	37.5	0.1	7.5	25100	20100	75400	106900	1.0E-4	0.26	0.67
5.06	5.59	0	10.44	2.7	0.67	41.0	0.1	11.0	56600	45300	169700	148600	1.0E-4	0.26	0.67
5.59	7.46	0	10.77	2.5	0.66	42.5	0.1	11.0	56600	52000	195100	172400	9.0E-5	0.26	0.67
7.46	9.35	0	11.02	2.2	0.57	42.0	0.1	11.0	62900	50300	188600	166100	1.0E-4	0.26	0.67
9.35	11.25	0	10.29	2.0	0.56	41.5	0.1	9.5	52600	45700	174300	153300	1.1E-4	0.26	0.67
11.25	13.17	0	10.29	1.9	0.52	41.0	0.1	9.5	60500	48400	181000	159000	1.0E-4	0.26	0.67
13.17	15.68	0	9.84	1.9	0.54	37.5	0.1	7.5	33600	26900	108800	117400	3.0E-4	0.28	0.67
15.68	17.55	0	9.84	1.7	0.54	37.5	0.1	7.5	33600	26900	108800	117400	3.0E-4	0.28	0.67

Note: All stiffness moduli are defined at a reference pressure $p_{ref} = 100$ kPa and stress dependency factor $m = 0.5$. In the Drainage column, 0 = drained.

Considering the relatively stiff response obtained from the WIP-FE model using the interpreted parameters, and the inherent uncertainty in the OCR estimation, an alternative interpretation assuming normally consolidated conditions (OCR=1) throughout the soil profile was also conducted. The alternative constitutive model parameters under normally consolidated conditions are summarized in Tables A.12 and A.13.

The results show good agreement with field data for both piles as illustrated in Figure A.2 and confirm the general trend observed in the main body of this thesis; namely that WIP models tend to underestimate the initial stiffness of impact-driven

monopiles installed in predominantly dense sandy soils, while providing accurate prediction for vibrated piles, where installation effects are usually limited.

Table A.12: Alternative HSsmall material model properties per soil layer for pile P1v of Cuxhaven according to the NC interpretation of this study

z_{Top} [m]	z_{Bot} [m]	Drainage [-]	γ' [kN/m^3]	OCR [-]	K_0 [-]	φ' [deg]	c' [kN/m^2]	ψ [deg]	E_{50}^{ref} [kN/m^2]	$E_{\text{oed}}^{\text{ref}}$ [kN/m^2]	$E_{\text{ur}}^{\text{ref}}$ [kN/m^2]	G_0^{ref} [kN/m^2]	$\gamma_{0.7}$ [-]	ν_{ur} [-]	R_{inter} [-]
0.00	0.32	0	17.37	1	0.35	40.5	0.1	10.5	24000	19200	72100	171800	2.0E-05	0.26	0.67
0.32	1.48	0	20.23	1	0.30	44.5	0.1	14.5	32200	25700	96500	235200	5.0E-05	0.23	0.67
1.48	3.11	0	20.20	1	0.32	42.5	0.1	12.5	62500	50000	187600	199100	9.0E-05	0.24	0.67
3.11	4.21	0	19.44	1	0.36	39.5	0.1	9.5	40400	32300	119900	140200	1.2E-04	0.26	0.67
4.21	5.13	0	8.61	1	0.39	37.5	0.1	13.5	9480	4720	28300	60200	2.6E-04	0.26	0.67
5.13	5.49	0	10.37	1	0.34	41.5	0.1	11.5	69800	55900	209500	184000	1.3E-04	0.25	0.67
5.49	7.26	0	10.86	1	0.32	42.8	0.1	11.0	71900	59100	212200	185500	1.5E-04	0.26	0.67
7.26	8.52	0	11.07	1	0.35	41.5	0.1	11.5	70400	56300	212000	185800	1.5E-04	0.26	0.67
8.52	10.71	0	10.20	1	0.34	39.5	0.1	9.5	60600	48400	185300	160100	2.0E-04	0.27	0.67
10.71	12.76	0	10.94	1	0.34	41.5	0.1	11.5	70300	56200	209000	185700	1.8E-04	0.25	0.67
12.76	14.17	0	11.37	1	0.32	42.5	0.1	12.5	76300	61000	228800	200400	1.7E-04	0.26	0.67
14.17	15.56	0	11.33	1	0.32	42.5	0.1	12.5	74900	60000	224300	197800	1.8E-04	0.27	0.67
15.56	17.99	0	11.21	1	0.30	42.5	0.1	12.5	70300	56300	209500	184000	2.3E-04	0.28	0.67
17.99	20.00	0	9.74	1	0.30	37.5	0.1	7.5	38900	31100	116700	127900	2.7E-04	0.28	0.67

Note: Missing values (–) denote parameters not defined for specific layers. Stiffness parameters are referenced at $p_{\text{ref}} = 100$ kPa. In the Drainage column, 0 = drained.

Table A.13: Alternative HSsmall material model properties per soil layer for pile P2h of Cuxhaven according to the NC interpretation of this study

z_{Top} [m]	z_{Bot} [m]	Drainage [-]	γ' [kN/m^3]	OCR [-]	K_0 [-]	φ' [deg]	c' [kN/m^2]	ψ [deg]	E_{50}^{ref} [kN/m^2]	$E_{\text{oed}}^{\text{ref}}$ [kN/m^2]	$E_{\text{ur}}^{\text{ref}}$ [kN/m^2]	G_0^{ref} [kN/m^2]	$\gamma_{0.7}$ [-]	ν_{ur} [-]	R_{inter} [-]
0.00	1.13	0	18.79	1	0.34	41.5	0.1	11.5	26100	20900	78300	187500	4.0E-05	0.25	0.67
1.13	2.72	0	20.17	1	0.32	42.5	0.1	12.5	51400	41200	154300	203800	8.0E-05	0.24	0.67
2.72	3.70	0	20.34	1	0.33	42.0	0.1	12.0	73100	58500	191000	239000	1.0E-04	0.24	0.67
3.70	5.06	0	9.13	1	0.38	38.0	0.1	8.0	29600	23700	88900	135500	1.6E-04	0.28	0.67
5.06	5.59	0	10.44	1	0.34	41.0	0.1	11.5	70800	56600	213200	186500	1.3E-04	0.25	0.67
5.59	7.46	0	11.17	1	0.31	43.5	0.1	13.5	80600	64400	241700	214800	1.2E-04	0.25	0.67
7.46	9.35	0	10.61	1	0.32	42.5	0.1	12.5	75700	60600	227200	208700	1.4E-04	0.25	0.67
9.35	11.25	0	10.61	1	0.34	41.0	0.1	11.0	67400	53900	206600	195200	1.7E-04	0.25	0.67
11.25	13.17	0	10.29	1	0.36	40.0	0.1	10.0	61100	48900	193800	159700	2.0E-04	0.27	0.67
13.17	14.00	0	10.94	1	0.34	41.5	0.1	11.5	69900	55900	209600	184100	1.8E-04	0.25	0.67
14.00	15.68	0	10.66	1	0.35	40.5	0.1	10.5	64500	51600	191400	169000	2.0E-04	0.26	0.67
15.68	17.55	0	9.84	1	0.38	38.0	0.1	8.0	44200	35300	132600	132600	2.6E-04	0.28	0.67
17.55	20.00	0	9.84	1	0.38	38.0	0.1	8.0	44200	35300	132500	132600	2.6E-04	0.28	0.67

Note: Missing values (–) denote parameters not defined for specific layers. Stiffness parameters are referenced at $p_{\text{ref}} = 100$ kPa. In the Drainage column, 0 = drained.

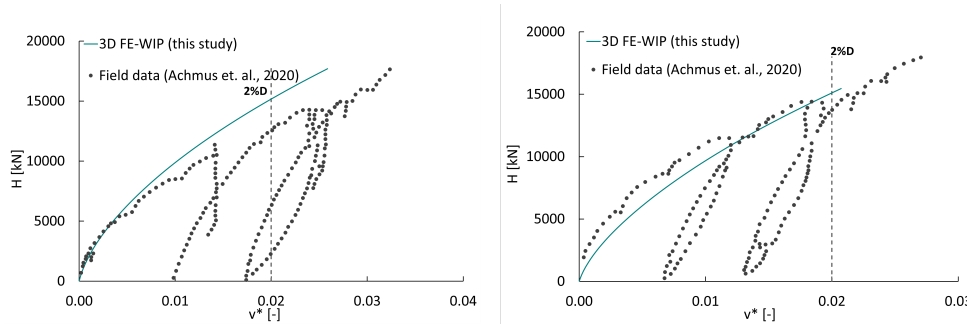

Figure A.2: Alternative load displacement curves for Cuxhaven piles, pile P1v (left) and P2h (right) assuming normally consolidated (NC) conditions

A.2.3 SIMOX model

The interpreted constitutive model parameters used for the SIMOX project are not disclosed in full due to confidentiality restrictions. Instead, a limited subset; namely OCR, K_0 and G_0 profiles, are given to investigate the effect of overconsolidation on the lateral response of piles 6A-V and 8B-H. Given the limited information on preconsolidation stress, a sensitivity study was conducted using three plausible values (25, 50 and 100 kPa) selected based on engineering judgement. The resulting variation in OCR, K_0 and G_0 profiles is illustrated in Figure A.3. An increased preconsolidation stress leads to higher OCR values, increased K_0 and ultimately increased G_0 through the pressure dependent formulation of HSsmall as described in Chapter 3 and shown in Equations 3.1 and 3.2.

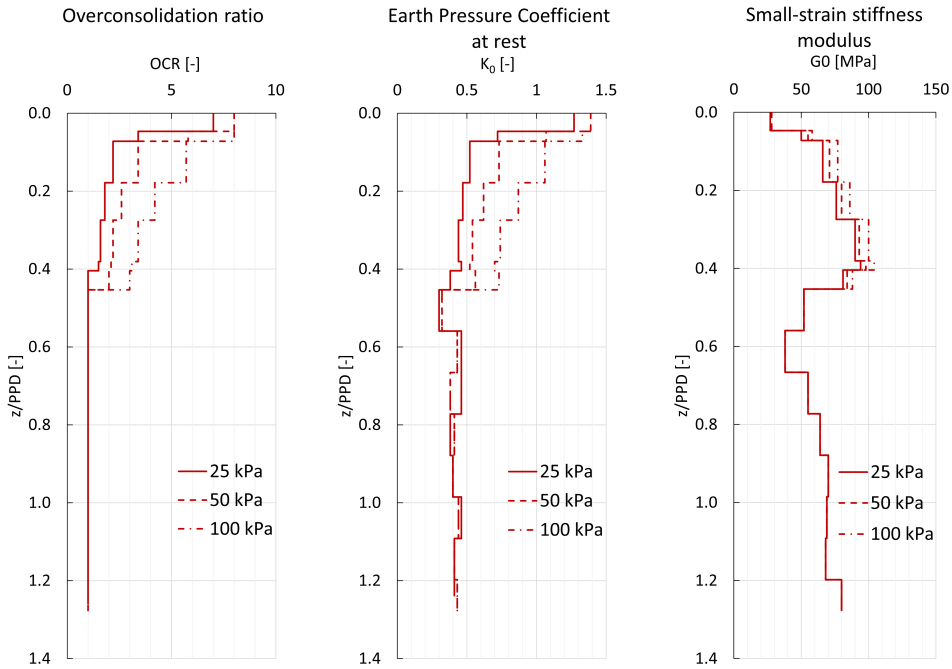

Figure A.3: Comparative OCR, K_0 and G_0 profiles for different preconsolidation stresses, for pile 6A-V of the SIMOX project

The effect of these three different overconsolidation profiles on the lateral response is shown in Figure A.4. The results show that even moderate changes in OCR - within the range of plausible values - can lead to variation in predicted stiffness and different level of agreement with the field test. The FE model with a preconsolidation pressure of 50 kPa yields the closest match with the field test and is therefore considered as the reference case for this study. Based on this study it is clear that accurate calibration of OCR is critical to avoid under- or overestimating initial stiffness and to match field observations.

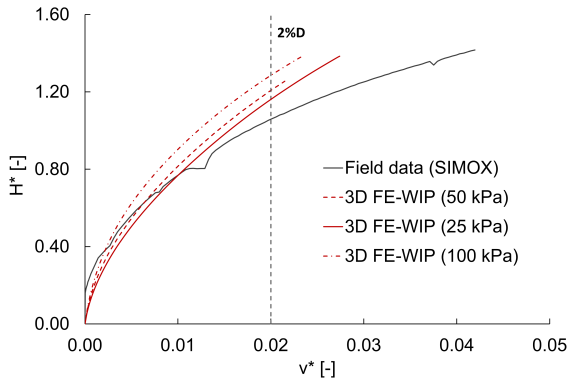

Figure A.4: Lateral load–displacement response of 6A-V for different OCR scenarios compared to field test

A.2.4 TU-Braunschweig (Stein) model

The constitutive model parameters for the tests of Stein [48] in overconsolidated sand are summarized in this section.

Table A.14: HSsmall material model properties for Z10 by Stein [48]

z_{Top} [m]	z_{Bot} [m]	γ' [kN/m^3]	OCR [-]	K_0 [-]	φ' [deg]	c' [kN/m^2]	ψ [deg]	E_{50}^{ref} [kN/m^2]	$E_{\text{oed}}^{\text{ref}}$ [kN/m^2]	$E_{\text{ur}}^{\text{ref}}$ [kN/m^2]	G_0^{ref} [kN/m^2]	$\gamma_{0.7}$ [-]	ν_{ur} [-]	R_{inter} [-]
0.00	0.36	7.00	5.0	1.07	35.5	0.1	5.5	19000	15200	57000	132000	2.0E-5	0.30	0.67
0.36	0.69	9.02	6.0	1.13	40.0	0.1	10.0	23300	18600	69800	165900	3.0E-5	0.26	0.67
0.69	1.03	9.74	3.8	0.81	42.0	0.1	12.0	24700	19700	74000	177800	3.0E-5	0.25	0.67
1.03	1.36	10.23	6.7	1.19	42.0	0.1	12.0	25200	20100	75500	181100	4.0E-5	0.25	0.67
1.36	1.69	10.66	5.3	0.99	43.0	0.1	13.0	37600	30100	112900	177800	5.0E-5	0.24	0.67
1.69	2.02	10.91	4.4	0.86	44.0	0.1	14.0	55200	44200	165600	198100	5.0E-5	0.24	0.67
2.02	2.38	10.99	5.2	0.98	43.0	0.1	13.0	67600	54100	202700	179700	6.0E-5	0.25	0.67
2.38	2.75	10.99	4.6	0.90	43.0	0.1	13.0	67700	54200	203200	180100	6.0E-5	0.24	0.67
2.75	3.00	10.99	4.6	0.90	43.0	0.1	13.0	67700	54200	203200	180100	6.0E-5	0.24	0.67

Note: All stiffness moduli are provided at reference pressure $p_{\text{ref}} = 100$ kPa and stress dependency factor $m = 0.5$. All layers are modelled as drained.

A.2.5 Case study model

Table A.15: HSsmall material model properties for the case study pile (CS1)

z_{Top} [m]	z_{Bot} [m]	Drainage [-]	γ' [kN/m^3]	OCR [-]	K_0 [-]	φ' [deg]	c' [kN/m^2]	s_u [kN/m^2]	ψ [deg]	E_{50}^{ref} [kN/m^2]	$E_{\text{oed}}^{\text{ref}}$ [kN/m^2]	$E_{\text{ur}}^{\text{ref}}$ [kN/m^2]	G_0^{ref} [kN/m^2]	$\gamma_{0.7}$ [-]	ν_{ur} [-]	R_{inter} [-]
0.00	1.70	0	8.8	1.0	0.34	40.9	0.1	–	17.8	51000	39000	153000	188000	0.00004	0.26	0.59
1.70	3.20	0	9.0	1.0	0.32	42.9	0.1	–	17.6	86000	62000	257000	216000	0.000047	0.24	0.59
3.20	8.10	0	9.0	1.0	0.28	46.0	0.1	–	17.9	129000	84000	387000	277000	0.000045	0.26	0.59
8.10	11.60	0	9.0	1.0	0.36	40.0	0.1	–	12.0	70000	55000	211000	222000	0.0001	0.26	0.59
11.60	14.40	2	8.6	4.1	0.81	15.0	15.0	136	0.0	31000	42000	92000	117000	0.0002	0.20	0.59
14.40	17.20	2	9.0	4.2	1.0	32.0	10.0	–	12.0	35000	49000	104000	137000	0.00025	0.26	0.59
17.20	18.20	2	9.0	2.1	0.58	15.0	15.0	116	0.0	35000	53000	103000	157000	0.0002	0.26	0.59
18.20	21.00	2	9.0	3.4	0.91	31.6	14	–	0.0	36000	52000	109000	147000	0.0002	0.32	0.59
21.00	28.80	2	9.0	3.5	0.91	31.9	12	–	0.0	47000	67000	142000	160000	0.0002	0.32	0.58
28.80	30.10	2	9.0	1.7	0.52	15.0	15.0	200	0.0	23000	34000	68000	156000	0.00034	0.20	0.58

Note: Missing values (–) denote parameters not defined for specific layers. Stiffness parameters are referenced at $p_{\text{ref}} = 100$ kPa. In the Drainage column, 0 = drained, 2 = undrained B

Appendix B

Finite Element Model

B.1 FE model definition

A parametric study was conducted in order to support the modelling decision (without modelling the pile toe and including the pile weight). The following figure illustrates that the effect of those two modelling parameters is negligible.

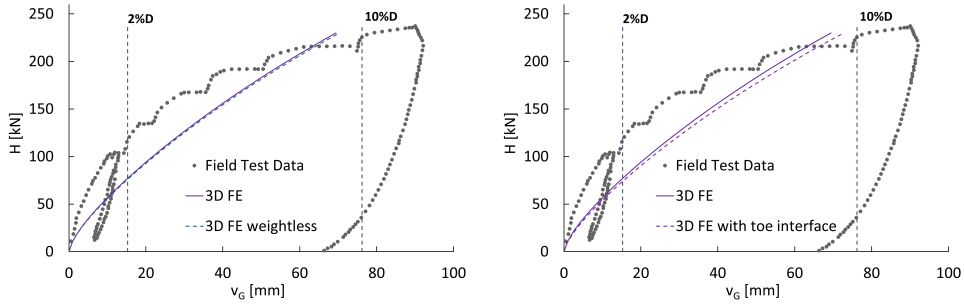

Figure B.1: Load displacement curves of pile PISA-DM4 to investigate the effect of weight (left) and pile toe modelling (right)

B.1.1 Mesh convergence study

To decide on the mesh quality a mesh convergence study was performed and it was found that an coarse mesh with approximately 27000 elements gives the best combination of accuracy and computational cost as compared to a fine mesh with 44547 elements for pile DL1 of PISA. Also refer to Fazlighiyasabadi et al. [24] who reports less than 2% change for a medium 37524 and fine 67406 elements test for the impact driven pile in Cuxhaven.

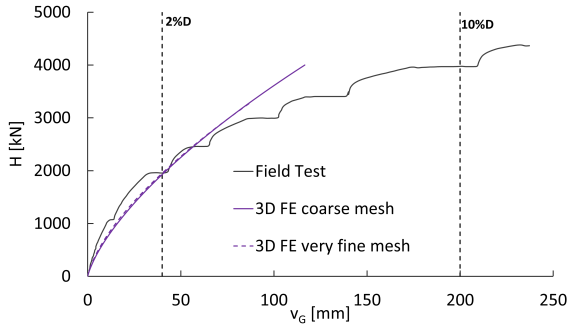

Figure B.2: Mesh convergence study results for PISA-DL1 pile

Appendix C

Installation Parameters

C.1 Post-installation soil state parameters

The parameters α and β of Equation 4.2 that were used per model and soil layer are summarized in this section.

z_{mid} [m]	q_c [MN/m^2]	D_r [%]	β [-]	α [-]	K_0^{post} [-]
0.18	1.49	72	0.20	0.43	2.72
0.53	5.55	95	0.20	0.46	3.02
0.86	10.67	105	0.15	0.48	3.39
1.20	14.84	104	0.15	0.47	5.71
1.53	19.01	110	0.15	0.46	5.41
1.86	22.11	114	0.15	0.44	5.38
2.20	24.97	111	0.15	0.43	7.00
2.57	24.97	109	0.15	0.39	7.33
2.88	24.97	109	0.15	0.37	8.08

Table C.1: Input parameters as a function of depth for the Stein-Z10 pile

Note that the post installation profile K_0 profile of SIMOX is considered more representative for the monopile dimensions that are used in offshore wind farms. However, verification against pressure measurements is still needed to draw a more informed conclusion. As also discussed above, the pile penetration depth (PPD) in the

z_{mid}/PPD	q_c [MN/m^2]	D_r [%]	β [-]	α [-]	K_0^{post} **[-]**
0.02	4.86	74	0.09	0.43	1.99
0.06	16.80	107	0.06	0.50	1.24
0.12	22.90	111	0.06	0.40	1.13
0.23	20.17	102	0.10	0.29	1.31
0.33	24.29	102	0.10	0.28	1.17
0.42	15.87	93	0.10	0.21	1.26
0.49	7.93	61	0.20	0.14	0.51
0.56	1.37	3	1.00	0.06	0.30
0.67	1.55	3	1.00	0.06	0.46
0.78	3.11	18	1.00	0.13	0.46
0.88	10.37	56	0.60	0.13	0.60
0.99	5.33	48	0.60	0.09	0.66
1.09	4.44	17	0.60	0.08	0.46

Table C.2: Input parameters as a function of normalized depth for pile 8B-H of SIMOX. Note that an average value for β was used for the transitional layer from unsaturated to saturated conditions.

z_{mid}/PPD	q_c [MN/m^2]	D_r [%]	β [-]	α [-]	K_0^{post} **[-]**
0.03	1.6	52	0.15	0.18	0.35
0.09	11.9	108	0.15	0.29	0.32
0.20	20.8	113	0.15	0.25	0.29
0.35	6.1	52	0.15	0.10	0.68
0.47	2.7	-	1.0	0.06	0.81
0.57	22.5	81	0.60	0.16	1.10
0.64	1.7	10	1.0	0.04	0.58
0.71	13.4	58	0.60	0.11	1.16
0.90	24.8	76	0.60	0.13	1.33
1.06	12.7	53	0.60	0.09	0.52

Table C.3: Input parameters as a function of normalized depth for the case study pile (CS1)

exponent of equation 4.2 defines the exponential decay of the horizontal stresses with depth due to friction fatigue. Therefore greater pile lengths and pile penetration depths imply more pronounced exponential decay therefore less increase in horizontal stresses and through equation 4.4 less increased $K_{0,mod}$.

TU Delft Delft University of Technology

SIEMENS energy